Differentiated rare-element mineralization in an ongonite – topazite composite dike at the Xianghualing tin district, Southern China: an electron-microprobe study on the evolution from niobium-tantalum-oxides to cassiterite

Fang-Fang Huang, Ru-Cheng Wang, Lei Xie, Jin-Chu Zhu, Saskia Erdmann, Xu-Dong Che, Rong-Qing Zhang

Differentiated rare-element mineralization in an ongonite–topazite composite dike at the Xianghualing tin district, Southern China: An electron-microprobe study on the evolution from niobium–tantalum-oxides to cassiterite

Fang-Fang Huang Ru-Cheng Wang , Lei Xie, Jin-Chu Zhu , Saskia Erdmann , Xu-Dong Che, Rong-Qing Zhang

Abstract

Our study characterizes in detail the mineralogical, textural and compositional features of a highly evolved, composite ongonite–topazite dike and its magmatic differentiation history. We present compositional data collected by established techniques, i.e. by electron microprobe and wet-chemical analysis, which provide a detailed framework for future studies that employ state-of-the-art analytical techniques. The studied dike (referred to as the No. 431 dike) crops out within the Xianghualing area in the Nanling Range of southern China, in close spatial association with Jurassic Sn–Nb–Ta granite plutons. The rock samples in the No. 431 dike were collected from a structurally lower drill hole and a trench at higher level. The ongonite is encountered throughout the dike, but the topazite is only revealed along the margin of the upper, near-surface dike. The results of whole-rock major and trace element analyses show that the rocks of the No. 431 dike are strongly peraluminous with an average ACNK value of ~ 1.5 for ongonite and > 3.9 for topazite. They are enriched in F, 1.7 wt.% and 5.4 wt.% on average for ongonite and topazite, respectively. The rocks have low Zr/Hf and Nb/Ta ratios, and high levels of ore-forming elements including Nb, Ta, Sn, and W. Silicate and oxide mineral assemblages, textures, and compositions are also distinct for the two rock types studied. In the lower ongonite of the dike, there are abundant phenocrysts of K-feldspar, quartz, and albite, and microphenocrysts of topaz and zinnwaldite in a matrix dominated by quartz, K-feldspar, and albite. Characteristic oxides are columbite–tantalite, tapiolite, and microlite, but cassiterite is absent. The upper ongonite of the dike has a silicate assemblage similar to the lower ongonite; columbite-(Mn), uranomicrolite, and limited amounts of cassiterite are the dominant accessory minerals. The topazite is characterized by large amounts of topaz and zinnwaldite intergrown with quartz, while K-feldspar, albite, and quartz phenocrysts have rounded shapes and are relatively rare. Cassiterite is the most abundant ore mineral, while Nb–Ta oxide minerals are less abundant. We interpret the whole-rock compositional trends, mineral textures, assemblages, and compositions to reflect the differentiation of an evolved, initially homogeneous magma that separated into aluminosilicate and hydrosaline melts, corresponding to crystallization of ongonite and topazite, respectively. The crystallization of Nb–Ta- and Sn-bearing ore minerals was strongly controlled by the separation of the two melt phases. We hypothesize that dike propagation/widening subsequent to the initial dike emplacement may have driven the separation of the aluminosilicate and hydrosaline melt phases that crystallized to ongonite in the core and topazite along the margins of the structurally higher part of the dike.

Keywords

- Ongonite;
- Topazite;
- Niobium–tantalum-oxides;
- Cassiterite;

- Nb–Ta–Sn mineralization;
- Fluorine;
- Fractional crystallization;
- Liquid immiscibility

1. Introduction

Ongonite and topazite, described frequently in the 1970s (Eadington and Nashar, 1978, Kovalenko et al., 1971 and Kovalenko et al., 1975), are two unusual types of felsic rock that are rich in rare elements. They are characterized by volcanic to shallow-intrusive textures, and abundant volatile-rich minerals (mainly topaz). Ongonite is defined as the phenocrystic subvolcanic analogue of granite that is rich in the rare elements Li and F (Kovalenko and Kovalenko, 1976). Topazite has been used in reference to felsic dikes that consist mainly of quartz and topaz, for which mineralogical, textural, and field relationships suggest a magmatic origin (Eadington and Nashar, 1978). Mineralization associated with these two particular types of rock has been described from many localities worldwide. Examples include W deposits associated with F-rich rhyolites (ongonites) from Ongon Khairkhan, Mongolia (Štemprok, 1991), the type locality of topaz rhyolite with W, Nb, Ta, and Sn mineralization (Burt, 1992), similar to topaz-albite granite, e.g., Limu in Southern China (Zhu et al., 2001), the French Massif Central (Cuney et al., 1992), Southern New Brunswick, Canada (Taylor, 1992), and the Eastern Desert, Egypt (Helba et al., 1997). The mineralization associated with topazite in Southern China is complex but dominated by Sn, such as deposits at Shicheng, Xunwu, Huichang, Yanbei and Taishun (Liu et al., 1996).

Although both ongonite and topazite are F-rich peraluminous rocks, their coexistence is not common. Kortemeier and Burt (1988) reported the first example of ongonite and topazite dikes occurring together in the Flying W Ranch area, Arizona, and they considered the rocks to be dominantly magmatic with fluorine-controlled transitions for both the ongonite and topazite, according to field, textural, mineralogical, and geochemical criteria. However, the ongonite and topazite in that area are not strongly mineralized.

The No. 431 dike in the Xianghualing tin district of southern China contains both ongonite and topazite in spatial association (Chen, 1984, Du and Huang, 1984, Zhu and Liu, 1990 and Zhu et al., 1993), and the typical mineralization involves Nb, Ta, and Sn. The coexistence of both ongonite and topazite in such a small-scale dike provides a unique opportunity to compare the rare-element mineralization in the two rock types. Our objective was to determine if the two rock types represent co-magmatic melts, and if so by which mechanisms they formed? Most interestingly, how can we explain the mineralization of these two different types of rock? We report comprehensive major and trace element whole-rock data, as well as detailed petrographic observations and mineral compositional data determined using electron microprobe analysis (EMPA). We evaluate the genetic relationship between ongonite and topazite exposed in a narrow dike, and discuss differentiation trends, particularly the coupled fractionation of F with Nb–Ta–Sn and the role of liquid immiscibility in their distribution between ongonite and topazite. We explore the potential role of oxides as an efficient container of rare metals and as a monitor of changes in fluid composition in mineralized highly-evolved silica systems. We believe that a detailed study of this kind provides an excellent framework for future investigations using advanced and new, evolving analytical techniques, particularly those targeting melt inclusions of the various mineral populations.

2. Geological setting and sampling of the Xianghualing No. 431 dike

The Xianghualing metallogenic district is located in the northern part of Linwu county, South Hunan province, which is in the center of the Nanling Range in South China. In terms of its tectonic setting, the Xianghualing district is situated where the middle part of the E–W-trending Nanling tectonic belt converges with the N–S-trending Leiyang–Linwu tectonic belt (Yuan et al., 2007). The Xianghualing district itself consists of a tectono-magmatic anticlinal dome that is composed mainly of Paleozoic strata with minor Mesozoic and Cenozoic strata. The main part of the lower Paleozoic consists of Cambrian arenaceous, argillaceous, and siliceous rocks together with minor carbonates. The upper Paleozoic strata lie unconformably on the lower Paleozoic, and are dominated by Middle Devonian conglomerates, sandstones, and shales of the Tiaomajian Formation (D_2t); Middle Devonian limestones and dolomites of the Qiziqiao Formation (D_2q); Upper Devonian dolomitic limestones and sandstones of the Shetianqiao Formation (D_3s); and Carboniferous carbonates and clastic rocks (Yuan et al., 2008).

Jurassic red beds and Cretaceous continental clastic rocks are found scattered in small basins in the northern and eastern parts of the district. Three early Yanshanian granite stocks have been identified in the area, and from south to north they are the Jianfengling granite (K–Ar age of 167 Ma; Mo et al., 1980), the Tongtianmiao granite, and the Laiziling granite (154–155 Ma, zircon U–Pb dating; Zhu et al., 2011). The mineralization associated with these granites includes W, Sn, Nb, Ta, Be, F, Pb, and Zn. This is also the type locality of hsianghualite, the first new mineral named by a Chinese mineralogist in China (Huang et al., 1958).

The No. 431 dike is located ~ 70 m northeast of the Laiziling granite (E112° 34′ 06″; N25° 27′ 26″) (Fig. 1). It is ~ 1770 m long and 1.8 to 18.0 m wide. The dike dips to the south at 42°–78°. The dike intrudes Devonian carbonates along a sharp contact, and the dike margins are characterized by flow structures and xenoliths of Devonian limestone which have chilled margins (Zhu and Liu, 1990). There is no direct evidence that the dike connects with the Laiziling granite body. However, vertical drilling has proved that the intrusive contact of the granite is inclined beneath the dike at an angle of 40°, and it thus seems possible that granite and the No. 431 dike are connected at depth.

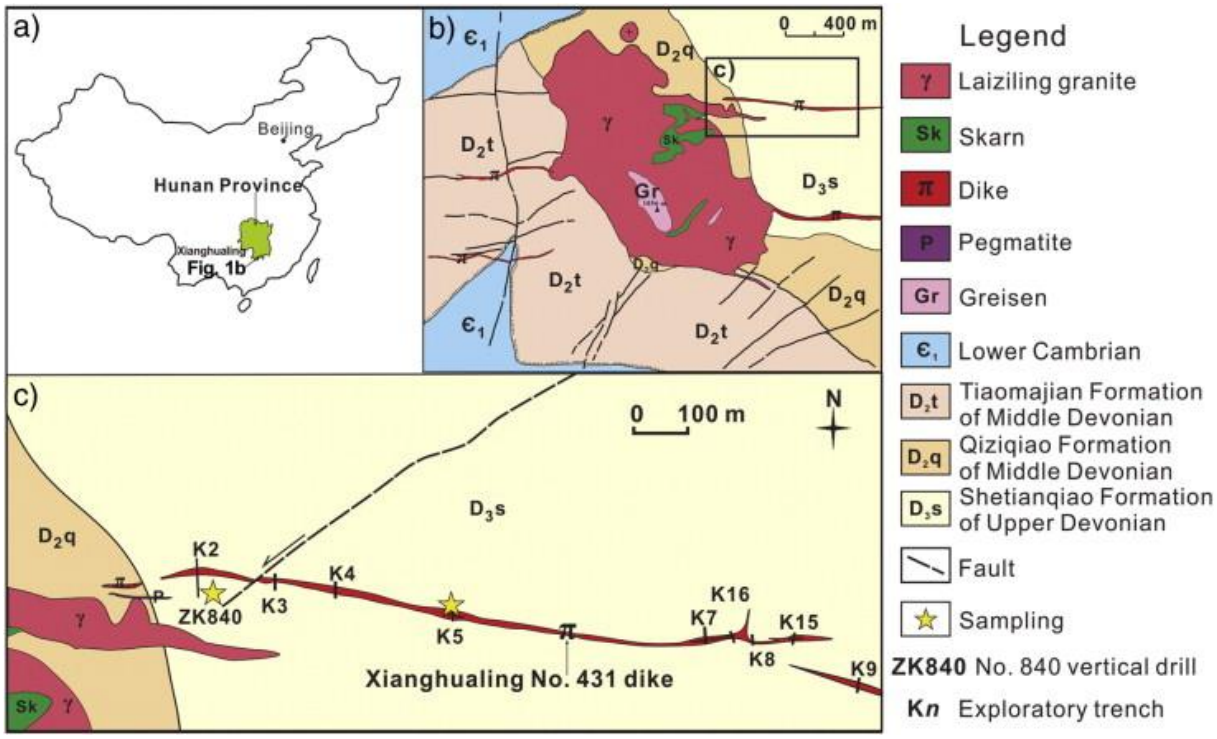

Fig. 1. : Simplified geological map of the No. 431 dike, Hunan Province, South China. (a) Location of Hunan Province in China; (b) the No. 431 dike in close spatial association to the ~ 154 –155 Ma Laiziling granite; and (c) the No. 431 dike sharply intrudes into carbonate-dominated strata.

Modified after Zhu et al., 2011

Ground (or near-surface) trenches and subsurface drillings were carried out in the early 1970s in order to investigate the dike. Earlier work had described the dike as heterogeneous, and it was classified as a topaz-bearing felsophyre and aplite (Du and Huang, 1984), but the later work of Zhu and Liu (1990) showed that the dike contains at least two major rock types, ongonite and topazite.

The samples we describe in this paper were collected from the No. 431 dike at two different locations. They capture the apparent petrographic variations both vertically and horizontally (Fig. 2). On the unexposed western side of the dike, the No. 840 drill revealed ongonite between depths of − 87.4 m and − 96.3 m. The samples acquired from the eastern side of the dike are exposed in the No. 5 exploratory trench. They contain spatially associated ongonite, occurring at the core of the upper dike, and topazite, occupying the marginal zones of the upper dike (Huang et al., 1988). Thus, ongonite appears throughout the dike, revealed both as lower ongonite in the subsurface drill hole and as upper ongonite in the near-surface trench, whereas topazite is only found in the upper part of the dike.

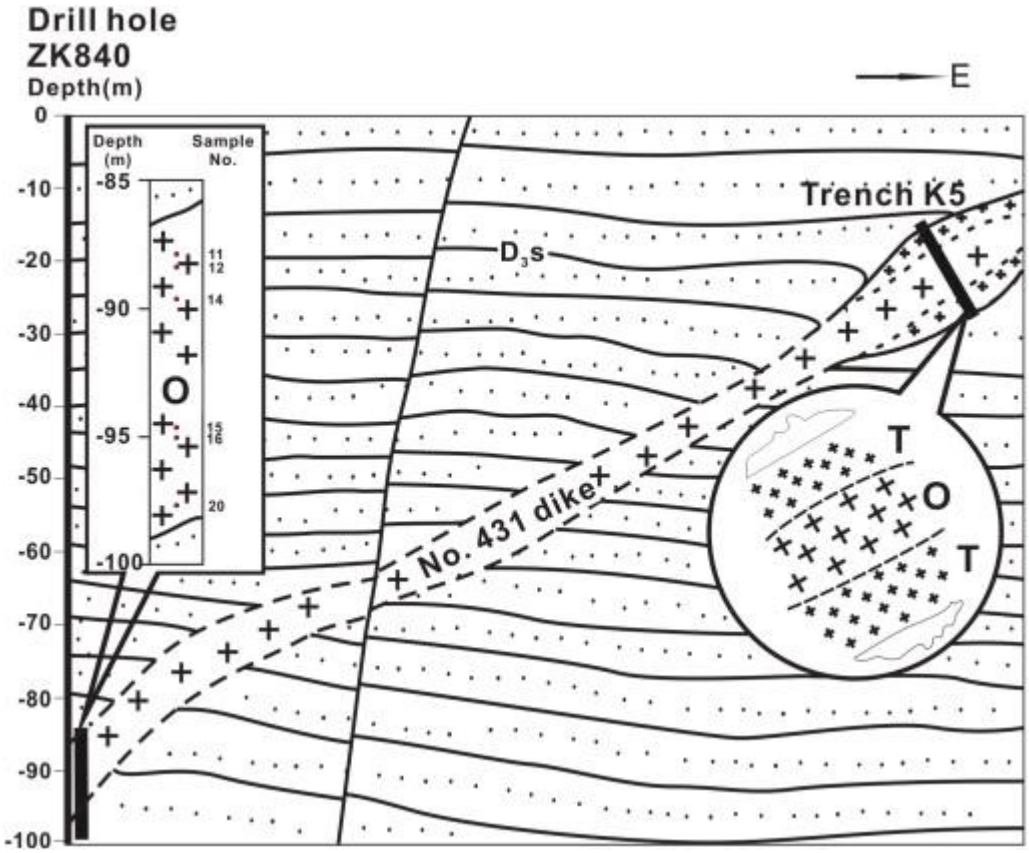

Fig. 2. : Cross-section of the No. 840 vertical drill hole and the No. 5 trench across the No. 431 dike. Abbreviations: O: ongonite; T: topazite

3. Analytical methods

In this study, we present new whole-rock geochemical data for 8 samples. Mineral assemblages and textures were characterized in 25 thin sections, while mineral compositions were determined for 14 selected samples. Whole-rock major-element compositions of the No. 431 dike were measured using wet-chemical analysis at the Analysis Center of the No. 230 Research Institute of the China National Nuclear Corporation (CNNC), Changsha, China. The following procedures were employed for determining various oxide contents: polyethylene oxide gravimetric methods for SiO_2; ethylene diamine tetra-acetic acid titration for Al_2O_3; the potassium dichromate volumetric method for Fe_2O_3; ethylene glycol tetra-acetic acid complexometric titration for CaO and MgO; hydrogen peroxide solution spectrophotometry for TiO_2; phosphomolybdenum blue spectrophotometry for P_2O_5; flame atomic absorption spectrophotometry for MnO_2; flame photometry for K_2O and Na_2O; and the potassium dichromate volumetric method for FeO. The ion selective electrode technique was used for determining F. The procedures are described in the Chinese National standard protocol GB/T 14506 (3-14)-2010. All the errors are less than 5%.

The analyses of trace and rare-earth elements were conducted with a Thermo X7 ICP-MS at the State Key Laboratory of Ore Deposit Geochemistry, Institute of Geochemistry, Chinese Academy of Science, Guiyang, China. For detailed information on the methods, see Qi et al. (2000).

Quantitative analyses of the minerals were guided by backscattered electron (BSE) images. The analyses were carried out on polished thin sections using a JEOL JXA-8100M electron microprobe (EMP) at the State Key Laboratory for Mineral Deposits Research of Nanjing University, China. The analyses were performed with a 15 kV accelerating voltage and 20 nA beam current, and with a beam diameter of 1 μm. Natural minerals (albite, fayalite, orthoclase, apatite, hornblende, topaz and scheelite) and synthetic metals (Nb, Ta and Sc metals) and compounds (UO_2, SnO_2 and $MnTiO_3$) were used as standards. For oxides, peak counting times were 10 s for Sn, 30 s for Ta and Nb, and 20 s for all other major elements, and for silicates the times were 30 s for Sn and W, and 10 s for all other major elements. All data were corrected using the ZAF correction procedures.

4. Petrography and geochemistry of the No. 431 dike

The No. 431 dike is composed of ongonite and mica-bearing topazite. All the ongonite specimens are white and they have a porphyritic texture (0.1–1.0 mm) with a fine-grained groundmass. Ongonite in the lower dike shows gradational zoning from a phenocryst-rich core zone to a phenocryst-poor topaz-bearing rim zone. In the upper dike, ongonite appears unzoned, while topazite shows fine-scale layers subparallel to the dike margin. The phenocrysts in the ongonites are mainly K-feldspar, quartz, albite, zinnwaldite, and rarely topaz. Their sizes may reach 1.5 mm; the groundmass consists mainly of albite, quartz, topaz, and minor zinnwaldite (Fig. 3a, b). Nevertheless, some differences exist between the ongonites in different parts of the dike. First, small amounts of anhedral fluorite have been found in the matrix of lower ongonite, while fluorite is very rare in upper ongonite. Second, although topaz appears in all the ongonites, it is short and prismatic in lower ongonite, and long and prismatic or needle-like in upper ongonite (Fig. 3c, d). The topazite, locally present at ground level, is composed mostly of topaz, quartz, and zinnwaldite that delineate a flow structure (Fig. 3e). The acicular topaz generally occurs in the interstices of anhedral quartz, and it is occasionally included in the quartz grains (Fig. 3f–h). The distribution of phenocrysts and matrix minerals from different rock types can be seen in Fig. 4.

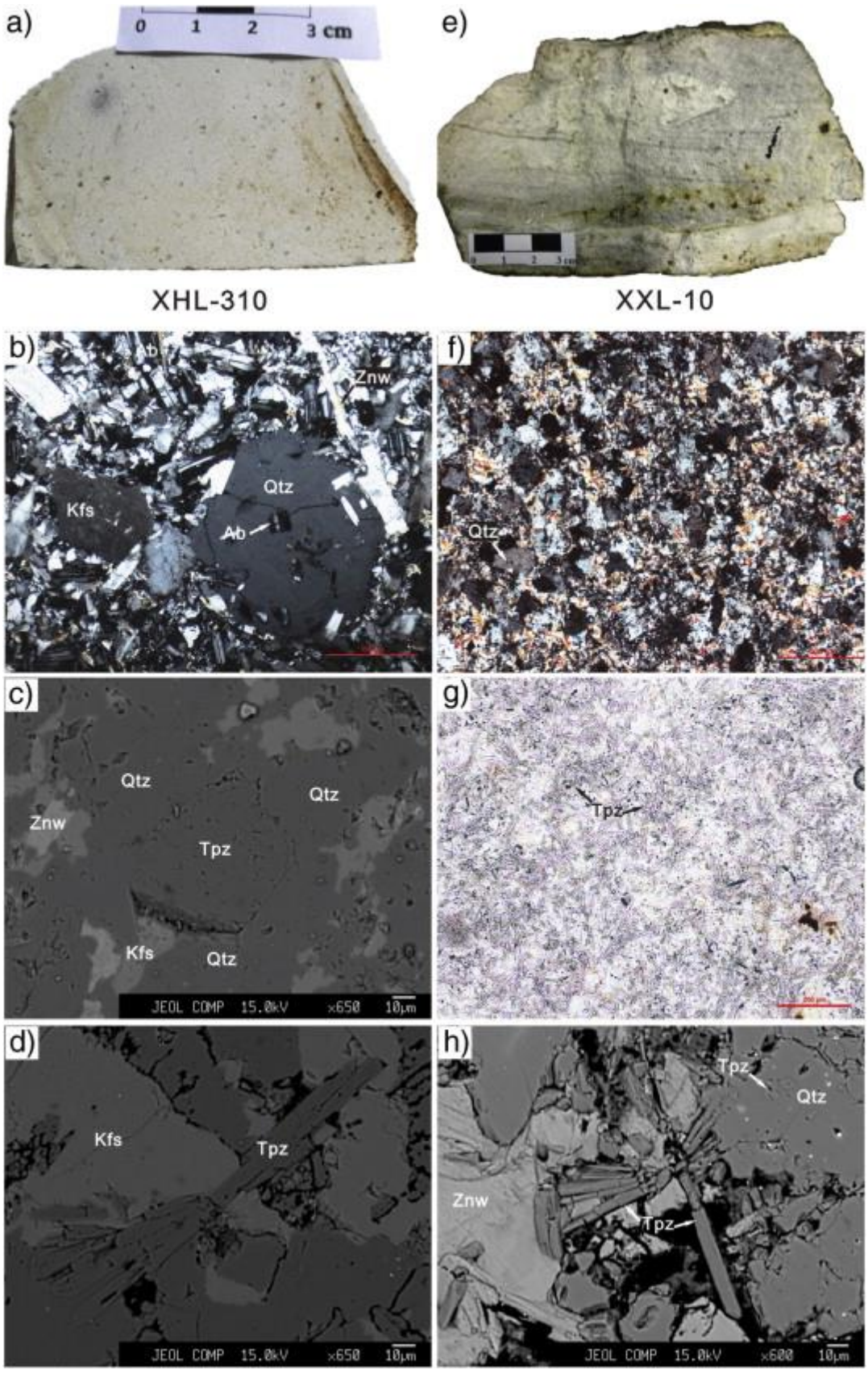

Fig. 3. : Photographs, photomicrographs, and BSE (back-scattered electron) images of ongonite and topazite. (a) Fine-grained upper ongonite with quartz phenocryst (gray); (b) quartz phenocryst in ongonite containing tabular albite crystals, under crossed polarized light; (c) short prismatic or columnar topaz in a groundmass of lower ongonite (BSE); (d) needle-like topaz in a groundmass of upper ongonite (BSE); (e) flow structure in fine-

grained topazite; (f) anhedral quartz and zinnwaldite in topazite, under crossed polarized light; (g) abundant acicular and high-relief topaz in topazite, under plane polarized light; and (h) needle-like topaz in topazite (BSE). Minerals abbreviations: Qtz: quartz; Ab: albite; Kfs: K-feldspar; Znw: zinnwaldite; Tpz: topaz.

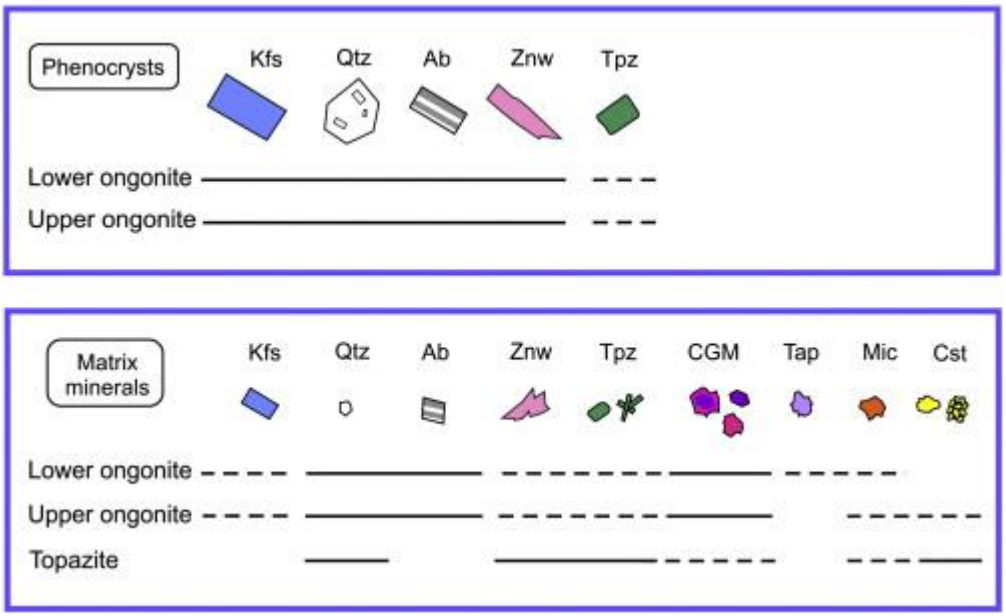

Fig. 4. : The distribution of phenocrysts and matrix minerals in ongonites and topazite from the No. 431 dike. Minerals abbreviations: CGM: columbite-group minerals. Solid line signifies abundant presence of minerals. Dashed line signifies rare occurrence of minerals.

Details of the whole-rock major and trace-element compositions of the No. 431 dike are given in Table 1. The data show that ongonites have similar compositions characterized by relatively high contents of SiO_2 (on average, 68.59 wt.%) and Al_2O_3 (on average, 18.47 wt.%), where SiO_2 contents decrease and Al_2O_3 contents increase from lower to upper parts of the dike. The rocks have a strongly peraluminous character with an average ACNK value of 1.5 [$Al_2O_3/(Na_2O + K_2O + CaO)$ in molars], and high F contents (on average, 1.7 wt.%). These characteristics are typical of ongonites elsewhere (Kovalenko and Kovalenko, 1976 and Štemprok, 1991). We further note that the marginal zone of lower ongonite (against the country rocks) is enriched in F and Li relative to its core zone (i.e., samples 10-11-20 versus samples 12-14; Table 1). Moreover, two slight differences in the major element contents between the lower and upper ongonites should not be ignored. Compared with ongonite in the near-surface, lower ongonite has higher contents of FeO_t and CaO (up to 3.03 and 1.00 wt.%, respectively), possibly corresponding to the higher mica and fluorite abundances. Relative to the ongonites, the topazite has a lower SiO_2 content, ranging from 56.57 to 63.08 wt.%, and higher Al_2O_3 content (up to 27.77 wt.%, average of 25.14 wt.%) and significantly higher F contents (up to 6.22 wt.%, average of 5.44 wt.%). The whole-rock SiO_2 content and FeO_t/MnO decrease from lower ongonite to upper ongonite and topazite in the No. 431 dike, while Al_2O_3 inversely increases (Table 1). Compared to the ongonite rocks, the Na_2O content of the topazite is extremely low (< 0.08 wt.% versus 3.80–6.88 wt.% for ongonites) while K_2O contents are relatively high, but variable (3.56–5.57 wt.% versus 1.05–4.59 wt.% for ongonites).

Table 1.

Major- and trace-element compositions of the Xianghualing No. 431 dike.

Rock type	**Lower ongonite**					**Upper ongonite**				**Topazite**			
Sample no.	**ZK840–**					**XXL–**		**XHL–**		**XXL–**			
	10*	**11***	**12***	**14***	**20***	**33**	**34**	**310**	**73**	**08**	**10**	**11**	**12**
SiO_2 (wt.%)	65.83	70.21	69.67	70.76	71.74	67.23	67.51	67.14	67.20	57.77	59.60	63.08	56.57
TiO_2						0.01	0.01	0.01	0.01	0.03	0.03	0.02	0.03
Al_2O_3	19.63	16.08	17.11	16.93	17.23	19.91	19.49	19.78	20.05	27.77	23.94	23.08	25.78
Fe_2O_3	0.44	0.40	0.29	0.10	0.42	0.17	0.02	0.02	0.02	0.44	1.07	0.36	1.68
FeO	2.63	2.66	1.73	0.79	0.55	0.14	0.26	0.15	0.22	0.92	2.14	1.15	2.08
MnO	0.06	0.06	0.04	0.03	0.02	0.03	0.08	0.09	0.08	0.83	0.47	0.36	0.49
MgO	0.16	0.30	0.14	0.12	0.62	0.01	0.01	0.02	0.01	0.11	0.08	0.04	0.05
CaO	0.49	0.57	0.71	0.70	1.00	0.03	0.02	0.02	0.05	0.04	0.03	0.01	0.03
Na_2O	4.00	3.80	6.88	5.70	4.52	4.54	4.54	4.80	4.13	0.08	0.07	0.06	0.07
K_2O	4.32	3.80	2.04	3.30	1.05	4.59	4.23	4.26	4.26	3.56	5.57	5.18	3.62
P_2O_5	0.00	0.00	0.01	0.00	0.00	0.01	0.03	0.02	0.02	0.01	0.01	0.02	0.01
Li_2O	0.21		0.18	0.13	0.05	0.31	0.45	0.48	0.54	1.47	1.67	1.38	1.49
H_2O	0.85	1.11	1.06	1.16	1.82								
LOI						2.13	2.74	2.49	3.06	5.99	4.73	4.61	7.34
F	3.30	2.32	1.20	1.16	2.06	1.11	1.19	1.42	1.34	4.99	5.18	5.36	6.22
Total	100.53	100.34	100.56	100.39	100.21	99.10	99.37	99.26	99.65	99.01	99.41	99.35	99.25
A/CNK	1.62	1.41	1.15	1.19	1.66	1.59	1.61	1.58	1.74	6.86	3.87	4.03	6.29
FeO_t	3.03	3.02	1.99	0.88	0.93	0.29	0.28	0.17	0.24	1.32	3.10	1.47	3.59
FeO_t/MnO	50.43	50.33	49.78	29.33	46.40	9.77	3.48	1.87	2.98	1.59	6.60	4.09	7.33
Li (ppm)		1230		886		765	958	1130	1450	6061	6110	5608	6252
Be		8.5		7.7		179	30	13	11	249	34	34	30
Sc		6.5		7.3		8.5	8.7	8.6	8.6	7.1	6.8	5.4	4.9
V		4.7		2.4		1.3	1.2	0.85	1.5	2.5	2.0	1.4	4.2
Cr		9.7		7.9		4.2	11	4.2	11	1.6	2.4	3.5	7.4
Cs		52		39		28	49	60	51	67	74	61	93
Rb		1418		1073		3880	4310	4670	4780	4918	5087	4440	4640
Ba		63		51		14	14	19	17	11	12	7.3	5.4
Th		6.6		6.3		20	11	15	10.0	39	27	30	23
U		25		15		9.5	4.9	7.4	6.9	18	6.9	20	11
Nb		149		248		97	99	133	105	223	105	193	163
Ta		57		175		114	65	97	69	207	100	175	161
Pb		42		30		140	106	52	40	180	139	193	58
Sr		59		78		11	14	15	8.2	16	13	32	12
Zr		71		18		46	30	32	35	77	4.2	86	70
Hf		16		3.2		7.7	3.9	5.7	5.1	22	0.69	24	19

Rock type	Lower ongonite					Upper ongonite				Topazite			
Sample no.	ZK840–					XXL–		XHL–		XXL–			
	10*	11*	12*	14*	20*	33	34	310	73	08	10	11	12
Y		1.7		1.4		0.34	0.35	0.30	0.44	0.54	0.18	0.33	0.57
Ga		59		66		57	55	53	59	25	41	24	33
Sn		35		13		18	38	63	29	142	438	247	802
W		4.6		5.5		39	25	69	24	114	60	758	771
La		1.5		4.5		1.9	2.5	2.5	1.4	2.1	1.0	1.9	1.5
Ce		5.5		17		5.2	6.9	6.2	4.0	5.2	3.8	5.8	3.9
Pr		0.73		1.7		0.52	0.70	0.65	0.40	0.70	0.44	0.67	0.53
Nd		1.8		3.4		0.97	1.3	1.2	0.85	1.6	0.86	1.1	1.2
Sm		0.55		0.88		0.26	0.34	0.29	0.31	0.34	0.16	0.19	0.23
Eu		0.03		0.02		0.02	0.02	0.02	0.02	0.05	0.02	0.01	0.02
Gd		0.32		0.47		0.12	0.14	0.12	0.16	0.13	0.06	0.09	0.15
Tb		0.09		0.08		0.04	0.04	0.03	0.05	0.04	0.02	0.02	0.02
Dy		0.60		0.56		0.27	0.21	0.21	0.34	0.22	0.06	0.10	0.15
Ho		0.11		0.11		0.05	0.04	0.04	0.06	0.05	0.02	0.02	0.03
Er		0.36		0.39		0.21	0.15	0.16	0.25	0.12	0.03	0.10	0.09
Tm		0.08		0.09		0.07	0.05	0.05	0.08	0.05	0.02	0.04	0.04
Yb		0.95		1.2		0.95	0.59	0.69	0.98	0.58	0.13	0.55	0.59
Lu		0.14		0.17		0.15	0.09	0.11	0.16	0.09	0.02	0.07	0.06
Nb/Ta		2.62		1.42		0.85	1.52	1.37	1.53	1.08	1.04	1.10	1.01
Zr/Hf		4.41		5.73		5.97	7.70	5.64	6.76	3.54	6.12	3.63	3.63
Rb/Sr		24.11		13.84		352.73	314.60	313.42	585.07	314.42	406.42	137.17	389.96
Total REE		12.76		30.06		10.72	13.01	12.24	9.07	11.26	6.67	10.68	8.61
LREE/HREE		3.80		8.90		4.77	8.96	7.66	3.36	7.92	17.38	9.71	6.52
δEu		0.20		0.08		0.30	0.24	0.26	0.23	0.70	0.55	0.24	0.37

Note: Major element of the samples with * is cited from Zhu et al. (1993); $FeO_t = FeO + Fe_2O_3 * 0.9$.

The samples from the No. 431 dike are enriched in Li, Rb, Cs, Nb, Ta, Be, Sn, W, and Hf, and depleted in Sr, Ba, P, and Ti, with significantly low Zr/Hf (on average 6.04 for ongonites and 4.23 for topazite) and Nb/Ta ratios (on average 1.55 for ongonites and 1.06 for topazite) (Table 1). The contents of the ore-forming elements Nb, Ta, Sn, and W are high, up to 248, 175, 62.6, and 68.5 ppm for the ongonites, and 223, 207, 802, and 771 ppm for the topazite, respectively. The contents of rare-earth elements (REE) in the ongonite and topazite samples are markedly low, and the normalized REE pattern is similar to the M tetrad effect of Takahashi et al. (2002) (Fig. 5). There are slight negative Eu anomalies; the δEu value for the ongonites and topazite average 0.22 and 0.47, and the $(La/Yb)_N$ ratio varies from 1.00 to 2.89 and 1.80 to 5.50, respectively.

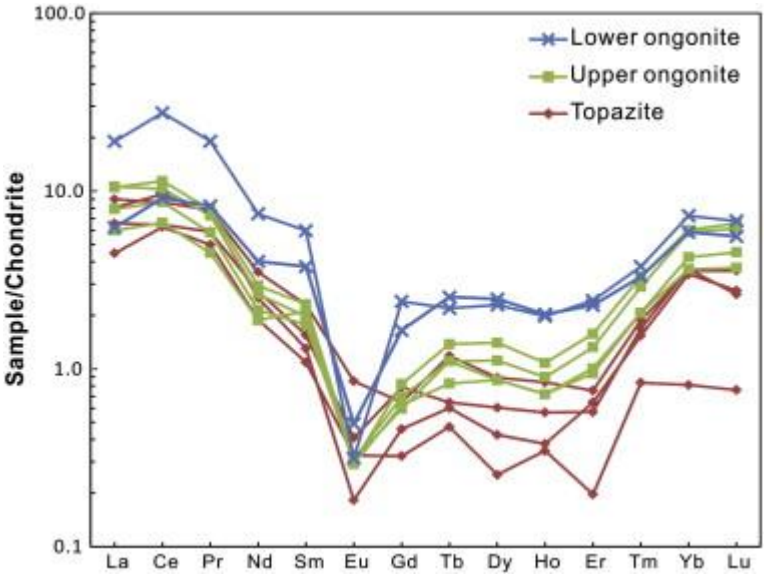

Fig. 5. : Chondrite-normalized REE patterns for the No. 431 dike (chondrite REE values from Anders and Grevesse, 1989).

5. Mineral chemistry

5.1. Feldspars

Feldspars, including K-feldspar and albite, are common in the ongonites but absent in the topazite. In the ongonites, K-feldspar exists mainly as subhedral phenocrysts up to 1 mm long, and locally it encloses albite. All K-feldspar has low Ab contents of 1.8–3.2 mol%. Albite occurs mostly as euhedral to subhedral tabular phenocrysts, but may also be included within K-feldspar or quartz to form a snowball texture which is usually observed in granites rich in rare-elements (Huang et al., 2002 and Pollard, 1989). Compositionally, the feldspars in the ongonites are nearly pure end members (K-feldspar has 1.79–3.18 mol% Ab, and albite has 97.00–99.1 mol% Ab) (Table 2).

Table 2.

Representative electron-microprobe results of feldspars and topaz in the Xianghualing No. 431 dike.

Rock type	**Ongonite**						**Topazite**	
	K-feldspar		**Albite**		**Topaz (matrix)**		**Topaz**	
Mineral	**Phenocryst**	**Phenocryst**	**Phenocryst**	**Matrix**	**Columnar**	**Acicular**	**Matrix**	**Phenocryst**
SiO_2 (wt.%)	62.80	63.55	69.08	68.79	31.47	31.38	32.30	32.40
TiO_2	–	–	–	–	–	–	–	0.01
Al_2O_3	18.40	18.38	20.51	20.17	57.76	56.30	55.92	55.50

Rock type	Ongonite						Topazite	
	K-feldspar		Albite		Topaz (matrix)		Topaz	
Mineral	Phenocryst	Phenocryst	Phenocryst	Matrix	Columnar	Acicular	Matrix	Phenocryst
MgO	0.02	–	–	–	–	0.03	–	–
CaO	–	0.00	0.13	0.01				
MnO	0.02	0.04	0.04	–	–	0.02	–	0.02
FeO	–	–	0.04	0.03	–	0.11	–	0.03
Na_2O	0.29	0.30	10.72	10.82				
K_2O	17.42	16.32	0.16	0.20	–	0.02	0.029	0.04
F					19.91	20.17	20.42	20.23
F═O					8.36	8.47	8.58	8.50
Total	98.94	98.60	100.68	100.01	100.76	99.55	100.07	99.76
Si (apfu)					0.948	0.963	0.987	0.994
Al					2.052	2.037	2.013	2.006
F					1.898	1.958	1.973	1.963
An	0.00	0.01	0.64	0.04				
Or	97.57	97.24	0.99	1.21				
Ab	2.43	2.75	98.37	98.75				

Note: –: Below detection limits; structural formulae of topaz were calculated on the basis of (Al + Si = 3).

5.2. Mica

In the ongonites, mica occurs as phenocrysts about 0.1 to 1.5 mm in size, and is also present in the groundmass. But it is not as abundant as in the topazite, and it is only locally found as one of main rock-forming minerals. According to electron-microprobe analyses, the micas in the ongonites and topazite mostly classify as zinnwaldite, together with minor lepidolite and rare lithian muscovite (following the classification of Foster, 1960a and Foster, 1960b). The FeO content of zinnwaldite in the lower ongonite may be up to 16.88 wt.%, while that in the upper ongonite from the trench is 6.62 wt.%, close to the composition of lepidolite. In contrast, the MnO content is highest in upper ongonite (up to 2.78 wt.% MnO), but very low in lower ongonite (only up to 0.95 wt.% MnO). Zinnwaldite from the topazite has FeO and MnO contents of about 10 wt.% and 1.9 wt.%, respectively, and the composition is similar to the micas in the coexisting ongonite. The F content of the zinnwaldite is on average 5.71 wt.% in lower ongonite from the drill hole, while in upper ongonite and topazite from the trench the values are higher, with averages of 8.89 wt.% and 8.17 wt.%, respectively (Table 3).

Table 3.

Representative electron-microprobe results of micas in the Xianghualing No. 431 dike.

Rock type	Lower ongonite			Upper ongonite			Topazite		
	1	**2**	**3**	**4**	**5**	**6**	**7**	**8**	**9**
SiO_2 (wt.%)	42.51	42.76	42.06	52.62	52.83	52.55	52.08	53.35	49.35
TiO_2	0.08	0.12	0.15	0.04	0.01	0.07	–	0.03	–
Al_2O_3	21.97	21.81	22.16	22.51	20.59	19.79	19.99	19.54	20.61
FeO	13.32	14.16	15.66	5.34	5.70	4.34	7.71	7.05	9.19
MnO	0.68	0.62	0.83	1.10	0.88	2.00	1.69	1.37	1.74
MgO	0.12	0.05	0.09	–	0.07	0.14	0.09	0.10	0.05
CaO	0.01	0.01	0.04	–	–	–	–	0.02	0.01
Na_2O	0.32	0.40	0.25	0.27	0.11	0.26	0.15	0.17	0.09
K_2O	10.00	10.09	9.28	10.82	9.22	11.03	10.41	9.67	10.28
Rb_2O	0.91	0.85	0.81	–	–	1.42	–	–	–
Cs_2O	0.04	0.02	0.04	–	–	0.04	0.02	–	0.01
F	6.35	7.85	6.14	8.58	8.36	8.45	8.04	8.28	7.92
F═O	2.67	3.31	2.58	3.61	3.52	3.56	3.39	3.49	3.33
Li_2O*	2.65	2.72	2.52	2.60	2.53	2.56	2.43	2.50	2.39
H_2O*	1.03	0.35	1.15	0.37	0.36	0.32	0.53	0.43	0.49
Total	97.30	98.48	98.58	100.63	97.13	99.40	99.75	99.02	98.80
Si	6.311	6.302	6.211	7.107	7.320	7.288	7.197	7.341	6.967
Al^{IV}	1.689	1.698	1.789	0.893	0.680	0.712	0.803	0.659	1.033
Al^{VI}	2.155	2.092	2.068	2.692	2.684	2.524	2.454	2.511	2.396
Ti	0.009	0.013	0.016	0.004	0.001	0.007	0.000	0.003	0.000
Fe	1.654	1.745	1.934	0.604	0.660	0.503	0.891	0.812	1.085
Mn	0.085	0.077	0.103	0.126	0.103	0.235	0.198	0.159	0.209
Mg	0.026	0.010	0.020	0.000	0.015	0.029	0.019	0.021	0.009
Li*	1.581	1.612	1.497	1.410	1.408	1.426	1.350	1.385	1.356
Sum oct	5.509	5.549	5.638	4.835	4.871	4.724	4.911	4.891	5.056
Ca	0.002	0.001	0.006	0.000	0.000	0.000	0.000	0.002	0.002
Na	0.093	0.114	0.071	0.070	0.031	0.070	0.040	0.045	0.025
K	1.893	1.897	1.747	1.864	1.629	1.951	1.836	1.696	1.852
Rb	0.087	0.080	0.077	0.000	0.000	0.126	0.000	0.000	0.000
Cs	0.002	0.001	0.002	0.000	0.000	0.003	0.001	0.000	0.001
Sum int	2.078	2.094	1.903	1.934	1.660	2.150	1.877	1.744	1.879
OH*	1.018	0.340	1.135	0.335	0.337	0.292	0.485	0.396	0.466
F	2.982	3.660	2.865	3.665	3.663	3.708	3.515	3.604	3.534
Al total	3.844	3.790	3.857	3.585	3.364	3.236	3.256	3.170	3.429
Fe/(Fe + Mg)	0.985	0.994	0.990	1.000	0.978	0.946	0.980	0.975	0.991

Note: –: Below detection limits. Structural formula calculated based on O = 23. *: LiO_2 and H_2O calculation of Fe-rich mica (Lower ongonite) and Fe-poor mica (upper ongonite and topazite) are after Tindle and Webb (1990) and Monier and Robert (1986), respectively.

5.3. Topaz

Topaz is only observed as an accessory mineral in the ongonites, but it is one of the main rock-forming minerals in topazite, where it can reach approximately 30 vol.%. Two kinds of topaz crystal are found in the ongonites of the dike: short prisms in lower ongonite and fine acicular crystals in upper ongonite. They usually coexist with other rock-forming minerals in the groundmass. In the topazite, topaz occurs dominantly as small grains in the groundmass, rarely as phenocrysts, but it also forms aggregates with cassiterite (see below). Radial arrays of needle-like topaz characterize the groundmass, of which some are included in quartz phenocrysts. In addition, EMPA results indicate that the topaz is fluorine-dominated with F contents of 18.88 to 21.67 wt.% (Table 2).

5.4. Niobium–tantalum oxides

Nb–Ta oxide minerals in the No. 431 dike include the columbite-group minerals which are always present, and the rarely observed tapiolite and microlite. The columbite-group minerals are present in all the ongonites and topazite to different degrees. Only a small amount of tapiolite is observed in lower ongonite, while microlite occurs in the ongonites as well as the topazite. Most of the Nb–Ta oxides are present in association with rock-forming minerals such as quartz, albite, and mica. Approximately 400 electron-microprobe analyses were obtained from about 80 Nb–Ta oxide grains in the studied ongonites and topazite, and representative results are presented in Table 4.

Table 4.

Representative electron-microprobe results of columbite-group minerals and tapiolite in the Xianghualing No. 431 dike.

Rock type	Lower ongonite												Upper ongonite					Topazite			
Mineral	Columbite-group minerals									Tapiolite			Columbite-group minerals					Columbite-group minerals			
	1	2	Range	3	4	Range	5	6	Range	7	8	Range	9	10	11	12	Range	13	14	15	Range
WO_3 (wt.%)	0.36	0.48	0.00–2.33	1.58	1.73	1.18–19.83	10.21	3.62	0.70–5.68	0.91	0.80	0.00–1.24	1.44	0.09	8.82	4.05	0.00–14.34	4.67	2.02	13.07	1.13–17.46
Nb_2O_5	62.54	67.64	38.40–74.55	28.59	35.02	20.73–45.93	23.34	25.09	22.83–28.05	5.54	8.42	4.82–12.62	65.41	41.93	32.55	47.82	28.20–65.49	37.96	40.38	33.89	33.89–44.83
Ta_2O_5	16.70	10.51	5.38–39.89	51.04	45.89	32.48–54.14	48.53	51.94	48.53–55.32	79.79	73.65	67.93–79.79	10.19	38.11	35.46	25.32	9.97–38.51	35.68	34.08	31.03	24.22–37.47
TiO_2	1.74	0.48	0.23–3.34	1.09	0.80	0.32–2.89	1.04	0.48	0.48–2.04	0.74	2.31	0.40–2.32	1.19	1.56	3.85	3.20	0.51–4.14	3.99	3.13	3.68	1.54–5.09
SnO_2	0.07	0.01	0.00–0.15	0.01	0.01	0.00–0.96	0.16	0.19	0.07–0.20	0.13	0.17	0.05–0.23	0.01	0.29	0.67	0.08	0.00–1.24	0.87	0.48	1.32	0.09–11.72
Sc_2O_3	0.67	0.16	0.12–2.27	0.59	0.09	0.01–0.80	–	0.29	0.00–0.29	–	–	0.00–0.20	0.27	1.24	1.14	0.82	0.22–1.26	0.68	1.26	1.07	0.30–2.56
MnO	11.13	13.13	8.09–14.55	5.74	4.77	3.01–10.67	3.72	3.99	3.28–7.99	0.51	0.55	0.41–0.59	12.00	15.44	16.53	18.02	10.95–18.85	15.97	16.76	14.45	13.23–17.48
FeO	5.80	8.37	6.43–10.87	12.11	12.67	6.57–15.58	13.36	14.83	11.16–14.83	14.02	14.18	13.83–16.48	9.62	1.38	0.96	1.39	0.67–9.62	0.49	1.33	1.93	0.40–6.51
Total	99.01	100.78		100.74	100.97		100.36	100.43		101.63	100.08		100.12	100.03	99.97	100.68		100.30	99.43	100.44	
W	0.006	0.007		0.029	0.030		0.191	0.067		0.019	0.016		0.022	0.001	0.152	0.065		0.079	0.034	0.222	
Nb	1.694	1.781		0.905	1.078		0.760	0.815		0.202	0.300		1.734	1.239	0.977	1.340		1.116	1.185	1.006	
Ta	0.272	0.166		0.973	0.850		0.950	1.015		1.746	1.578		0.163	0.677	0.640	0.427		0.631	0.602	0.554	
Ti	0.078	0.021		0.057	0.041		0.056	0.026		0.044	0.137		0.053	0.077	0.192	0.149		0.195	0.153	0.182	
Sn	0.002	0.000		0.000	0.000		0.005	0.005		0.004	0.005		0.000	0.008	0.018	0.002		0.023	0.012	0.034	
Sc	0.035	0.008		0.036	0.006		0.000	0.018		0.000	0.000		0.014	0.071	0.066	0.044		0.038	0.071	0.061	
Mn	0.565	0.648		0.341	0.275		0.227	0.242		0.035	0.037		0.596	0.855	0.930	0.946		0.879	0.922	0.804	
Fe	0.291	0.408		0.710	0.722		0.804	0.891		0.943	0.934		0.472	0.075	0.053	0.072		0.027	0.072	0.106	
Mn/(Fe + Mn)	0.66	0.61	0.46–	0.32	0.28	0.17–	0.22	0.21	0.20–	0.04	0.04	0.03–	0.56	0.92	0.95	0.93	0.55–	0.97	0.93	0.88	0.68–

Rock type	Lower ongonite												Upper ongonite					Topazite			
Mineral	Columbite-group minerals									Tapiolite			Columbite-group minerals					Columbite-group minerals			
	1	2	Range	3	4	Range	5	6	Range	7	8	Range	9	10	11	12	Range	13	14	15	Range
			0.70			0.62			0.42			0.04					0.96				0.98
Ta/(Nb + Ta)	0.14	0.09	0.04–0.38	0.52	0.44	0.30–0.58	0.56	0.55	0.52–0.58	0.90	0.84	0.76–0.91	0.09	0.35	0.40	0.24	0.09–0.41	0.36	0.34	0.36	0.25–0.39

Note: –: Below detection limits. 1, 2 are the representative results of the columbite-(Mn) core; 3, 4 are the representative results of the columbite-(Fe) or tantalite-(Fe) rim; 5, 6 are the representative results of the tantalite-(Fe) associated with tapiolite.

5.4.1. Niobium–tantalum oxides in ongonite of the lower dike

Columbite-group minerals appear in lower ongonite of the dike mostly as fine grains less than 300 μm in size, which are commonly interstitial to the rock-forming minerals. Sometimes the columbite contains inclusions of quartz and topaz, indicating its simultaneous crystallization with those rock-forming minerals (Fig. 6). Progressive zoning is occasionally observed in some crystals, characterized by increasing brightness in BSE images (Fig. 6a). In particular, the grains commonly display < 20 μm wide, very bright rims (Fig. 6a, b). Electron-microprobe results indicate that the columbite-group minerals can be divided into two groups on the basis of their compositions. The dominant part in some zoned crystals displays variations in Mn/(Fe + Mn) (shortened hereafter as $Mn^{\#}$) from 0.46 to 0.70, and in Ta/(Nb + Ta) (shortened to $Ta^{\#}$) from 0.04 to 0.38. Overall, most of them fall into the field of columbite-(Mn) (Table 4; Fig. 6e). The brightest outermost parts of the grains are tantalite-(Fe) or Ta-rich columbite-(Fe). They have moderate $Ta^{\#}$ of 0.30–0.58 and a variable $Mn^{\#}$ of 0.17–0.62.

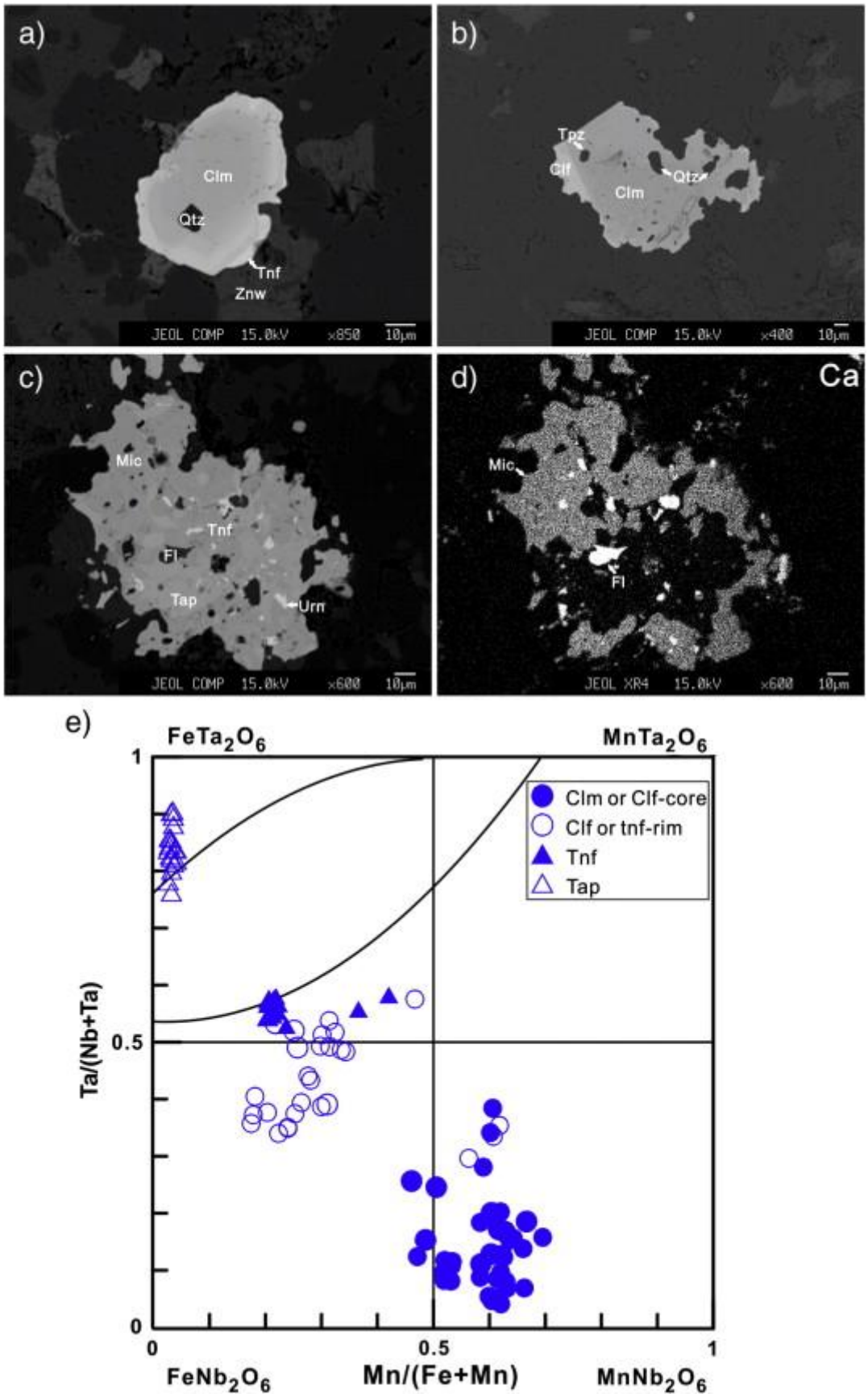
a)
Clm
Qtz
Tnf
Znw
JEOL COMP 15.0kV ×850 10μm
b)
Tpz
Clf
Clm
Qtz
JEOL COMP 15.0kV ×400 10μm
c)
Mic
Tnf
Fl
Tap
Urn
JEOL COMP 15.0kV ×600 10μm
d)
Ca
Mic
Fl
JEOL XR4 15.0kV ×600 10μm
e)
FeTa2O6
MnTa2O6
Clm or Clf-core
Clf or tnf-rim
Tnf
Tap
Ta/(Nb+Ta)
1
0.5
0
0
0.5
1
FeNb2O6
Mn/(Fe+Mn)
MnNb2O6

Fig. 6.

BSE images and compositional classification of the columbite-group minerals and tapiolite from the ongonite of the lower dike. (a) Progressive zoning of columbite-(Mn) core with a rim of tantalite-(Fe); (b) columbite-(Mn) core and columbite-(Fe) rim with topaz and quartz inclusions; (c) microgranular aggregate of columbite-group minerals, tapiolite, and microlite; (d) X-ray scanning map showing the Ca distribution of (c); and (e) compositions of the columbite-group minerals and tapiolite from lower ongonite, plotted on the Mn/(Fe + Mn) versus Ta/(Nb + Ta) quadrilateral diagram. Minerals abbreviations: Clf: columbite-(Fe); Clm: columbite-(Mn); Tnf: tantalite-(Fe); Tap: tapiolite-(Fe); Mic: microlite; Urn: uraninite; Fl: fluorite.

Microgranular aggregates in the marginal zone of lower ongonite make up the second-most important occurrence of Nb–Ta oxide minerals. Back-scattered electron images demonstrate that tantalite-(Fe) and tapiolite are the main minerals in the centers of the aggregates, and these are surrounded by many irregular microlite grains (Fig. 6c, d). Uraninite and fluorite may also be found in this complex association. The results of the analyses of tantalite-(Fe) show a restricted $Ta^{\#}$ ranging from 0.52 to 0.58 and a $Mn^{\#}$ ranging from 0.20 to 0.42. They plot precisely near the bottom boundary of the miscibility gap between tantalite and tapiolite (Černý et al., 1992). Tapiolite, a kind of highly Fe-dominated Ta-enriched oxide, has extremely high values of $Ta^{\#}$ and low values of $Mn^{\#}$, ranging from 0.76 to 0.91 and 0.03 to 0.04, respectively. Its composition plots close to the top boundary of the miscibility gap (Fig. 6e). The third main mineral in the aggregates is microlite, containing 8.69 wt.% Na_2O, 5.54 wt.% CaO, and 6.23 wt.% UO_2 on average (Table 5). In addition, the fluorine content of the microlite in subsurface ongonite is up to 4.23 wt.%, the highest of all the microlites from the different rocks of this dike.

Table 5.

Representative electron-microprobe results of microlite in Xianghualing No. 431 dike.

Rock type	**Lower ongonite**			**Upper ongonite**			**Topazite**		
	1	**2**	**3**	**4**	**5**	**6**	**7**	**8**	**9**
Nb_2O_5 (wt.%)	10.41	16.21	3.93	5.64	7.63	7.25	7.38	7.62	13.06
Ta_2O_5	62.25	53.14	73.30	66.81	63.23	57.80	60.48	59.34	56.06
TiO_2	0.73	0.61	0.27	1.26	1.33	1.18	1.07	1.62	3.45
Na_2O	7.70	9.22	8.50	0.20	0.28	0.11	7.41	7.62	13.06
CaO	6.23	5.28	5.62	3.28	2.18	1.54	3.50	3.96	3.22
MnO	–	–	0.01	0.20	0.57	0.38	0.18	0.13	0.46
FeO	0.03	0.09	0.05	0.25	0.38	0.81	0.23	0.41	0.09
UO_2	6.97	6.91	4.26	12.71	13.61	13.22	12.48	12.50	17.46
PbO	0.39	0.48	0.26	0.33	0.66	6.56	0.39	0.38	0.56
WO_3	–	1.43	0.30	0.75	1.24	1.62	1.09	0.65	0.73
SnO_2	0.26	0.18	0.15	0.32	0.25	0.34	0.33	0.28	0.34
Sc_2O_3	1.09	0.96	1.09	1.25	0.91	1.03	1.01	1.06	0.50
F	3.15	3.35	3.96	2.70	1.81	1.01	2.24	2.40	1.50
F═O	1.33	1.41	1.67	1.14	0.76	0.42	0.94	1.01	0.63

Rock type	Lower ongonite			Upper ongonite			Topazite		
	1	**2**	**3**	**4**	**5**	**6**	**7**	**8**	**9**
Total	97.89	96.43	100.02	94.55	93.31	92.42	96.84	95.26	97.55
B site									
Nb	0.424	0.648	0.162	0.233	0.314	0.323	0.320	0.329	0.493
Ta	1.526	1.279	1.813	1.662	1.566	1.548	1.576	1.539	1.274
W	0.000	0.033	0.007	0.018	0.029	0.041	0.027	0.016	0.016
Ti	0.050	0.041	0.018	0.087	0.091	0.087	0.077	0.116	0.217
A site									
Na	1.346	1.581	1.498	0.036	0.049	0.021	1.376	1.409	2.116
Ca	0.602	0.501	0.547	0.322	0.212	0.163	0.359	0.404	0.288
U	0.140	0.136	0.086	0.259	0.276	0.290	0.266	0.265	0.325
Pb	0.010	0.011	0.006	0.008	0.016	0.174	0.010	0.010	0.013
Mn	0.000	0.000	0.000	0.005	0.015	0.010	0.005	0.003	0.011
Fe	0.003	0.007	0.004	0.019	0.029	0.067	0.019	0.033	0.007
Sc	0.086	0.074	0.086	0.099	0.072	0.088	0.084	0.088	0.036
Sn	0.009	0.006	0.006	0.012	0.009	0.014	0.012	0.011	0.011
F	0.897	0.937	1.140	0.781	0.521	0.314	0.679	0.724	0.395

Note: –: Below detection limits. Structural formulae based on Nb + Ta + W + Ti = 2.

In summary, the Nb–Ta oxides display an overall Ta dominance toward the marginal zones of lower ongonite of the dike, especially for the structurally highest level, characterized first by the appearance of Ta-dominated minerals such as tapiolite and microlite, and second by the overall increasing $Ta^{\#}$ value in the columbite, as revealed in Fig. 7.

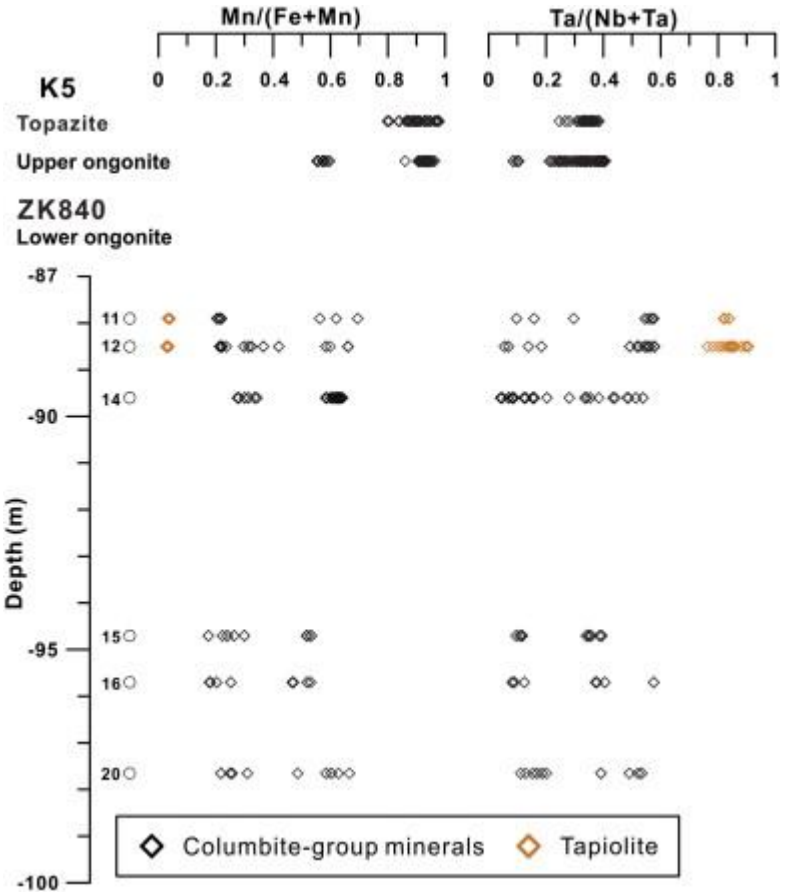

Fig. 7. : Chemical variations of the columbite-group minerals and tapiolite from lower ongonite, upper ongonite and topazite.

5.4.2. Niobium–tantalum oxides in ongonite of the upper dike

In comparison with the lower ongonite of the dike, the columbite-group minerals in upper ongonite are compositionally simpler. Intergranular subhedral tabular crystals up to 100 μm long (Fig. 8a) that contain low $Ta^{\#}$ values of 0.09 to 0.11 and $Mn^{\#}$ values of 0.55 to 0.60 classify as columbite-(Mn) (Table 4). Moreover, abundant subhedral to anhedral fine-grained crystals occur interstitially in near-surface ongonite, and they have moderate $Ta^{\#}$ values of 0.21 to 0.41 and high $Mn^{\#}$ values of 0.86 to 0.96. This type of columbite also classifies as columbite-(Mn). The columbite-(Mn) is characteristically enriched in tungsten with a maximum of 18.86 wt.% WO_3 and an average of 4.54 wt.%. The third type of columbite grains is part of a mineral association that includes microlite (Fig. 8b) and/or rutile + zircon, and these grains are commonly 10–50 μm in size. They have distinctively high values of $Ta^{\#}$ and $Mn^{\#}$, ranging from 0.32 to 0.37 and 0.91 to 0.94, respectively. All the columbite group minerals found in upper ongonite are columbite-(Mn), and the latter two kinds of Nb–Ta oxide minerals share close positions in the columbite–tantalite quadrilateral diagram (Fig. 8c). The associated microlite is characterized by high UO_2 contents up to 15.36 wt.% but low Na_2O and CaO levels. It could therefore be classified as uranomicrolite according to the classification suggested by Hogarth (1977) and Černý (1989).

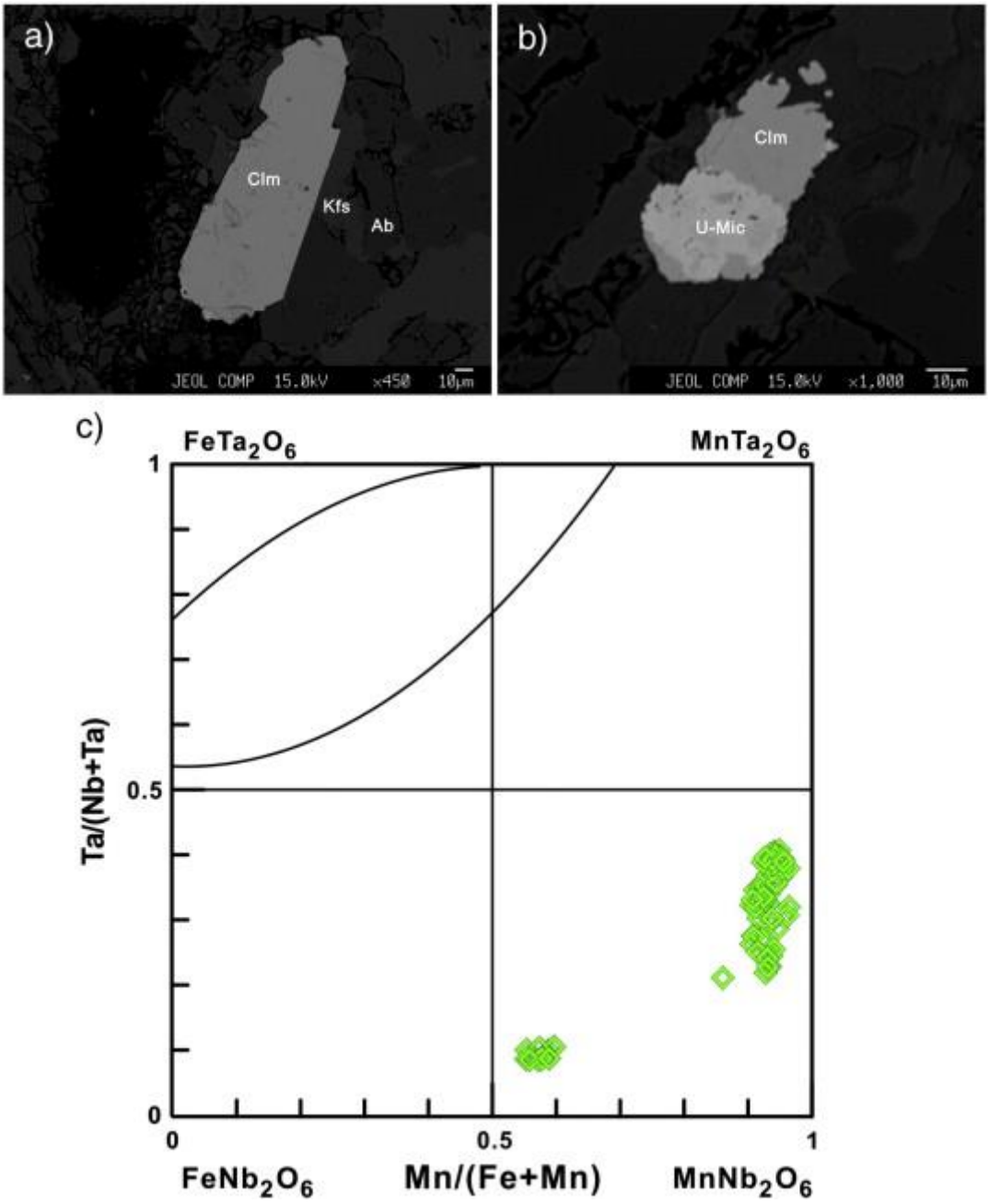

Fig. 8. : BSE images and compositional classification of the columbite-group minerals from the ongonite of the upper dike. (a) Euhedral tabular columbite-(Mn) is interstitial to the rock-forming minerals, (b) columbite-(Mn) intergrowth with U-rich microlite, and (c) compositions of the columbite-group minerals from upper ongonite, plotted on the Mn/(Fe + Mn) versus Ta/(Nb + Ta) quadrilateral diagram. Minerals abbreviations: U-Mic: uranomicrolite.

Tantalian rutiles are only found in upper ongonite as euhedral–subhedral crystals in aggregates of Nb–Ta oxide minerals, and they contain up to 21.92 wt.% Ta_2O_5 and trace amounts of Fe, Mn, Sn, and W.

5.4.3. Niobium–tantalum oxides in topazite

In the topazite, columbite-group minerals are fewer and smaller in size (10–15 × 10–30 μm), and they commonly occur as subhedral crystals associated with microlite or hubnerite

(Fig. 9a, b). Chemical analyses show that the columbite-group minerals also correspond to columbite-(Mn) in the classification diagram (Fig. 9c). Overall the $Ta^{\#}$ and $Mn^{\#}$ values of columbite-(Mn) in topazite overlap those in the associated upper ongonite. Subhedral to anhedral microlite is present along with the columbite-(Mn), and it is rich in uranium with up to 17.46 wt.% UO_2, which means it can be classified as an uranomicrolite. The association of columbite and microlite is consistent with the assemblage observed in the spatially associated ongonite.

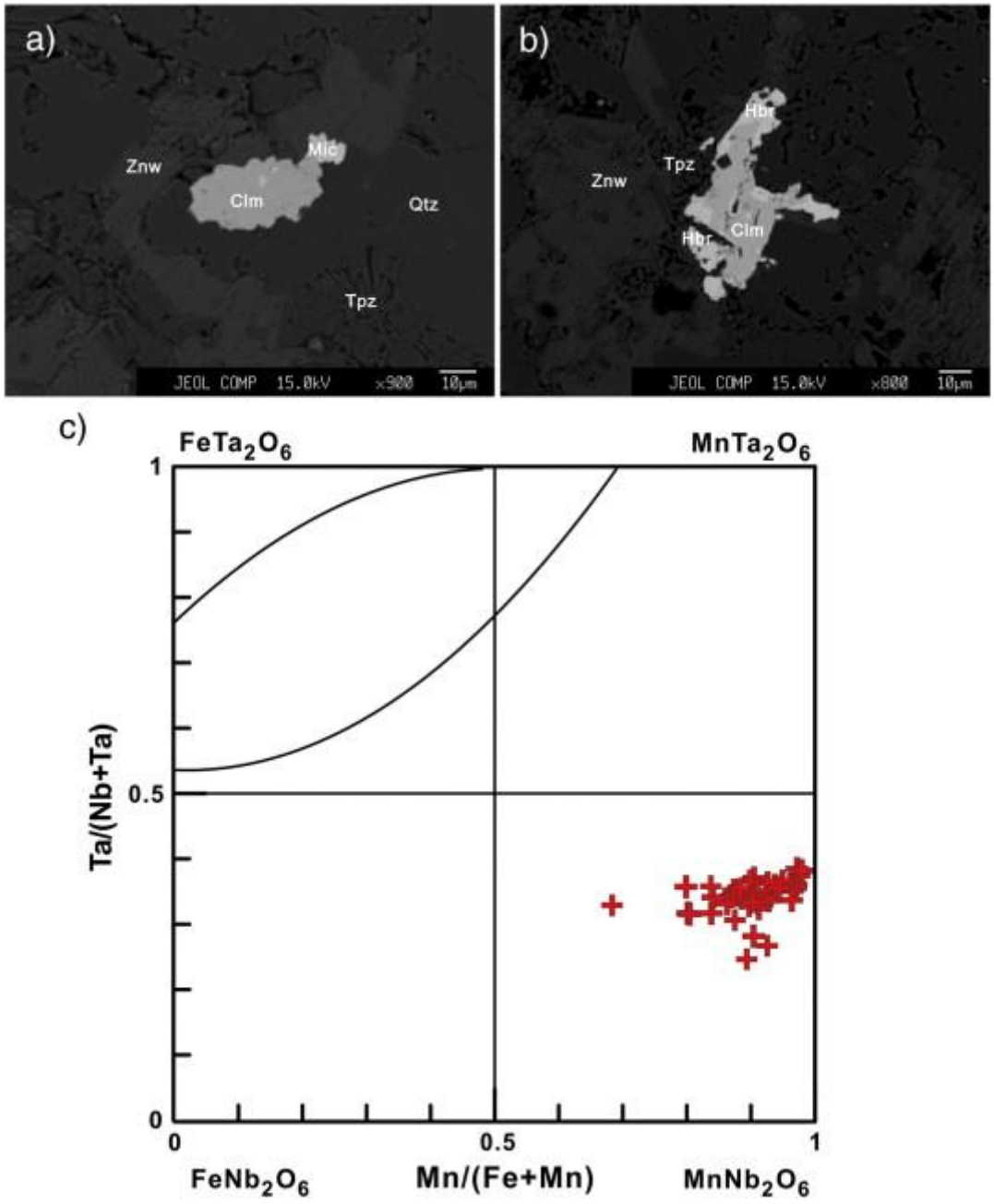

Fig. 9. : BSE images and compositional classification of the columbite-group minerals from topazite of the upper dike. (a) Fine-grained columbite-(Mn) intergrown with U-rich microlite, interstitial to the rock-forming minerals; (b) subhedral columbite-(Mn) intergrown with hubnerite; and (c) compositions of the columbite-group minerals from topazite, plotted on the Mn/(Fe + Mn) versus Ta/(Nb + Ta) quadrilateral diagram.

5.5. Cassiterite

Cassiterite is almost absent in lower ongonite and scarce in upper ongonite. It occurs as anhedral crystals or fine veinlets along zinnwaldite cleavages. In contrast, in the topazite, cassiterite is abundant as an accessory mineral. According to the textural evidence and mineral compositions, two main types of cassiterite may be distinguished in the topazite: disseminated and aggregated cassiterites, and they are considered below (Table 6; Fig. 10).

able 6.

Representative electron-microprobe results of cassiterites in the Xianghualing No. 431 dike.

Rock type	**Upper ongonite**				**Topazite**							
	Cassiterite				**Disseminated cassiterite**				**Aggregated cassiterite**			
Mineral	**1**	**2**	**Average n = 20**	**SD**	**3**	**4**	**Average n = 41**	**SD**	**5**	**6**	**Average n = 32**	**SD**
WO_3 (wt.%)	0.83	0.11	0.22	0.39	–	1.82	0.88	1.04	0.18	0.04	0.21	0.47
Nb_2O_5	0.37	0.04	0.14	0.18	0.20	2.63	1.26	1.08	0.07	0.01	0.11	0.18
Ta_2O_5	0.04	–	0.34	0.48	2.33	5.83	3.04	1.75	0.51	0.03	0.17	0.30
TiO_2	0.19	–	0.22	0.36	0.18	0.62	0.31	0.36	0.09	–	0.16	0.28
SnO_2	98.35	99.73	98.32	1.42	97.44	87.37	92.42	4.16	98.12	99.23	98.13	1.24
Sc_2O_3	–	–	0.01	0.02	–	0.08	0.03	0.04	0.02	–	0.01	0.03
MnO	0.09	0.01	0.03	0.04	0.04	0.70	0.24	0.29	–	–	0.05	0.08
FeO	0.38	0.08	0.20	0.15	0.18	1.87	1.42	1.01	0.11	0.05	0.22	0.26
Total	100.24	99.97	99.48		100.38	100.93	99.60		99.09	99.37	99.07	
W	0.005	0.001	0.001		0.000	0.012	0.006		0.001	0.000	0.001	
Nb	0.002	0.000	0.001		0.001	0.015	0.007		0.000	0.000	0.001	
Ta	0.000	0.000	0.001		0.008	0.020	0.011		0.002	0.000	0.001	
Ti	0.004	0.000	0.004		0.003	0.012	0.006		0.002	0.000	0.003	

Rock type	Upper ongonite				Topazite							
	Cassiterite				Disseminated cassiterite				Aggregated cassiterite			
Mineral	1	2	Average n = 20	SD	3	4	Average n = 41	SD	5	6	Average n = 32	SD
Sn	0.981	0.998	0.987		0.973	0.877	0.934		0.990	0.999	0.990	
Sc	0.000	0.000	0.000		0.000	0.001	0.000		0.000	0.000	0.000	
Mn	0.002	0.000	0.001		0.001	0.015	0.005		0.000	0.000	0.001	
Fe	0.004	0.001	0.002		0.002	0.017	0.013		0.001	0.000	0.002	

Note: –: Below detection limits. The number of cations is calculated on the basis of 2 atoms of oxygen.

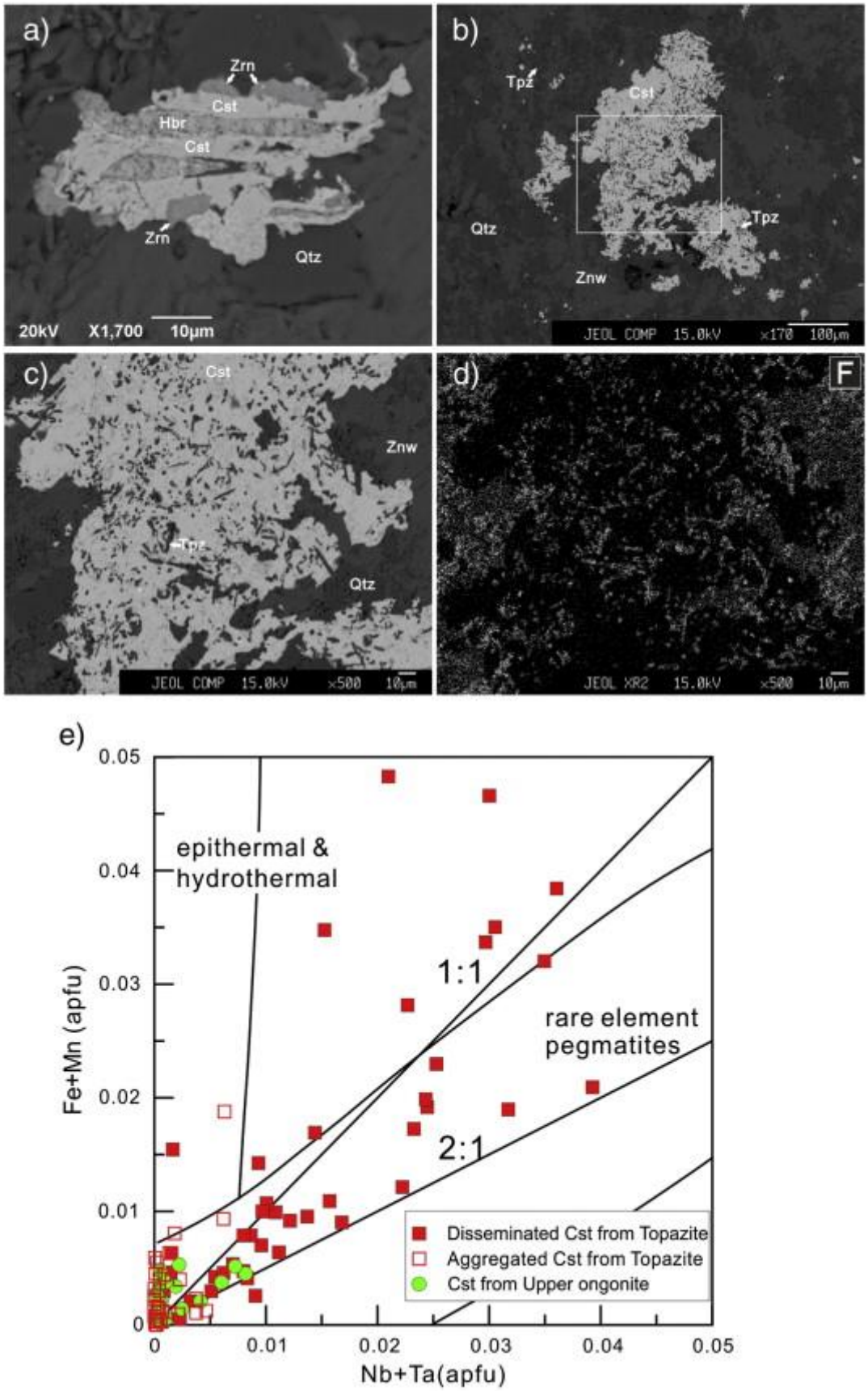

Fig. 10. : BSE images and covariation diagram of (Nb + Ta) vs. (Fe + Mn) in cassiterite from ongonite and topazite in the upper dike. (a) Disseminated cassiterite intergrown with hubnerite and zircon; (b) aggregates of cassiterite intergrown with abundant topaz; (c) enlargement of part of (b) showing

aggregates of cassiterite intergrown with abundant topaz; (d) X-ray scanning map showing the distribution of F of (b); and (e) covariation diagram of (Nb + Ta) vs. (Fe + Mn) for cassiterite from upper ongonite and topazite. Minerals abbreviations: Cst: cassiterite; Hbr: hubnerite; Zrn: zircon.

After Tindle and Breaks, 1998.

(1) Disseminated cassiterite occurs as independent euhedral to subhedral granular crystals (10–20 μm across), either in the interstices between topaz and quartz, or in a mineral association with zircon, columbite-(Mn), hubnerite, and/or microlite (Fig. 10a). The composition of this type cassiterite is similar to that of magmatic cassiterite in pegmatites rich in rare metals (Černý, 1989 and Neiva, 1996), and it is characterized by significant amounts of Ta (up to 7.77 wt.% Ta_2O_5), Nb (up to 4.01 wt.% Nb_2O_5), and W (up to 5.13 wt.% WO_3), together with minor Mn (up to 1.34 wt.% MnO) and Fe (up to 3.89 wt.% FeO). In the Nb + Ta vs. Fe + Mn diagram, disseminated cassiterite is mostly dispersed along the 2:1 line, corresponding to the general substitution of columbite solid-solution in cassiterite: $3Sn^{4+} \Leftrightarrow 2(Nb, Ta)^{5+} + (Fe, Mn)^{2+}$, similar to that described by Černý and Ercit (1989) and Tindle and Breaks (1998).

(2) Aggregated cassiterite is typically present as micron-sized crystals in aggregates with needle-like topaz (Fig. 10b–d). This type of cassiterite has low levels of trace elements (less than 1 wt.%) (Fig. 10e). Moreover, minor amount of galena is locally found included in cassiterite aggregates, suggesting their crystallization was part of a later hydrothermal process.

5.6. Varlamoffite

Varlamoffite is a hydrous Sn mineral only found in the topazite. It usually occurs in cavities, and occasionally it is associated with cassiterite. It contains 44.55 wt.% SnO_2 and 23.18 wt.% FeO, on average, and probably about 30 wt.% H_2O.

6. Discussion

In this part, we first discuss the magmatic fractionation of the composite ongonite–topazite dike using mineral assemblages and their textures as well as whole-rock compositional data. We then evaluate mineral-scale textural and compositional evidence for the fractionation of the volatile and incompatible elements F and Nb–Ta–Sn. Lastly, we discuss mechanisms that may have driven the spatial segregation of magmas that crystallized to ongonite and topazite.

6.1. Co-magmatic relationships between ongonite and topazite in the Xianghualing No. 431 dike

Although both ongonite and topazite have equivalents among granitic rocks that are rich in rare elements, their coexistence was only described in 1988 from the Flying W Ranch of Arizona (Kortemeier and Burt, 1988). In addition, Johnston and Chappell (1992) also described co-magmatic, topaz-bearing aplite (very similar to ongonite) and topazite. They suggested their co-magmatic origin on the basis of petrographic investigations, in spite of their presence in different dikes. The Xianghualing No. 431 dike exposes coexisting ongonite and topazite in a very small scale dike (less than 18 m wide). The ongonite and topazite of the No. 431 dike have highly evolved compositions with ~ 1.1–6.2 wt.% F, ~ 750–6250 ppm Li, and an ACNK index of > 1.1 to ~ 6.9, where the degree of differentiation increases from

lower ongonite over upper ongonite to associated topazite. Additionally, both Nb/Ta and Zr/Hf ratios decrease in the same order. Compositionally, the ongonite and topazite rocks are very similar to F-rich, peraluminous, highly evolved, and volatile-rich eruptive rocks such as the Macusani glass in SE Peru (Pichavant et al., 1987) and topaz rhyolites (Breiter, 2012, Gioncada et al., 2014, Raimbault and Burnol, 1998 and Xie et al., 2013). Other topazites (Songling, Hailuoling, Tongkengzhang, Fenghuangdong and Yangbin) besides the Xianghualing No. 431 dike in southern China also share similar petrological and geochemical characteristics (Liu et al., 1996). Most of them contain quartz and topaz as the rock-forming minerals and occasionally have fine-grained zinnwaldite. They are generally relatively rich in SiO_2, strongly peraluminous and have a high content of F (up to 6.55 wt.%) (Liu et al., 1996). Trace elements of topazites are rich in HFSE (Nb, Ta, Sn, W, Zr and Hf) with high values of Rb/Sr and low values of Zr/Hf and Nb/Ta.

How the evolved magma emplaced in the No. 431 dike crystallized and how the ongonite types and topazite are related to each other are discussed in the following sections, using the compositional variation and the distribution of mineral assemblages, their textures, and composition. The main features we seek to explain are: (i) the strong increase in F, Li, Sn, and W and the decrease in Na_2O from ongonite to topazite in the upper dike; (ii) the highly porphyritic texture of ongonites throughout the dike; (iii) the euhedral–subhedral phenocrysts in core zone of the lower ongonite and upper ongonite, and the subrounded phenocrysts in marginal zone of the lower ongonite and the topazite; and (iv) the highly contrasting abundance and mineral textures of topaz, Nb–Ta oxide minerals, and cassiterite in ongonite and topazite (Fig. 4).

Studies of natural examples and experimental results have demonstrated that liquid immiscibility may play an important role in the evolution volatile-rich magmatic system and particularly in the evolution of Li–F-rich granitic magmas (e.g., Kamenetsky and Kamenetsky, 2010, Peretyazhko et al., 2007, Roedder, 1992, Roedder and Coombs, 1967, Shchekina et al., 2013, Veksler, 2004 and Veksler et al., 2012). High concentrations of alkali and earth alkali metals favor liquid immiscibility and high concentrations of non-silicate anions (e.g., F^-, CO_3^{2-}) permit their efficient separation. Low-pressure (72 –100 MPa), high-temperature (650–1100 °C) experiments performed by Veksler et al. (2012) have revealed that in immiscible silicate–fluoride systems, the fluoride melt strongly partitions F, Li_2O, MgO, and CaO and moderately partitions Al_2O_3, Na_2O, and K_2O. Trace elements that most strongly partition into the fluoride melt are W, Th, and the REEs. Additionally, in carbonate–silicate systems, the carbonate liquid strongly partitions Na_2O and CaO and moderately partitions K_2O, Mo, and W.

The strong and abrupt increase in the concentrations of F and Li from ongonite to topazite and the increase in MgO from the upper ongonite to coexisting topazite in the No. 431 dike is thus consistent with unmixing of silicate and fluorite melts. The very low Na_2O content and the variable K_2O content of the topazite samples in the margin of the dike are not only suggested by the experimental silicate–fluoride partition coefficients, but could also reflect the unmixing of carbonate species, as the dike wall rocks are dominated by carbonate strata. Trace-element partitioning could have also been governed by carbonate and fluorine species, as they seem to most strongly partition the ore minerals Nb, Ta, Sn, and W that are strongly enriched in the topazite of the No. 431 dike.

The presence of the phenocrysts of K-feldspar, quartz, albite, zinnwaldite, minor topaz and columbite-(Mn) – in the structurally lower part (ongonite in the subsurface, lower part of the

dike; Fig. 11a, b) and also in the near-surface part of the dike – suggests that early crystallization enriched the melt phase in elements including the network-modifiers Li and F and ore elements Sn and W (Time 1, ongonite in the near-surface, upper part of the dike, Fig. 11c, d). The large size of the phenocrysts in ongonite indicates that crystal nucleation was slow relative to crystal growth (e.g., Hersum and Marsh, 2007 and Pietro, 2008). Such crystallization is consistent with the presence of large amounts of volatiles and other network-modifiers and/or extended crystallization time (Fenn, 1977 and Swanson, 1977).

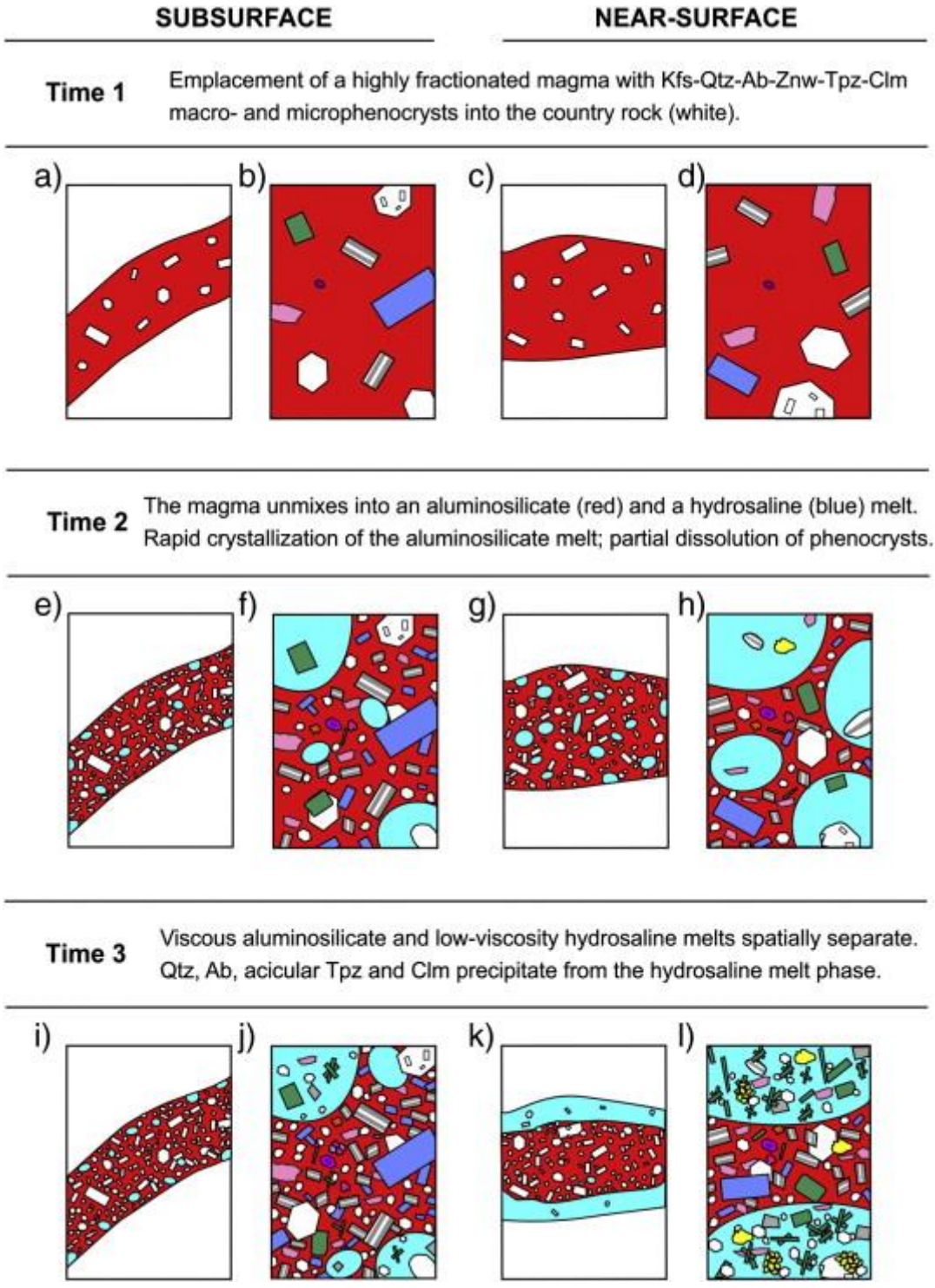

Fig. 11. : The proposed magmatic evolution of the No. 431 dike now exposed at subsurface and near-surface locations. Crystallization of an initially homogeneous, highly differentiated magma was

followed by unmixing of silicate- and fluoride-dominated melt phases that crystallized to ongonite and topazite, respectively.

In contrast, the strongly porphyritic texture of ongonites with abundant fine-grained quartz and albite along with K-feldspar, zinnwaldite, topaz, and ore minerals is consistent with subsequent rapid crystallization (e.g., Fig. 3b). Such rapid crystallization is typically invoked to be triggered by supercooling as a function of decreasing temperature and/or the exsolution of volatile components from an originally homogeneous melt phase (e.g., Breiter et al., 2005, Cobbing et al., 1986, London and Morgan, 2012 and Štemprok et al., 2008). Crystallization as a result of abrupt cooling alone is inconsistent with the occurrence of the most fractionated rocks, the topazite, along the margins of the No. 431 dike. Consistent with the compositional variation between ongonite and topazite rocks, we suggest that the fine-grained assemblage started to form when the granitic magma separated into aluminosilicate and hydrosaline melt phases that later crystallized ongonite and topazite lithologies, respectively (Time 2, Fig. 11e–h).

Once the two melt phases had unmixed (Time 3), the low-viscosity hydrosaline melts appear to have segregated from the more viscous aluminosilicate melt toward the margin of the dike (Fig. 11i–l). Possible driving forces for this segregation are discussed in the following section. Rare, subrounded silicate phenocrysts both in the rim zone of lower ongonite and in topazite were likely entrained from the assemblage that crystallized from the originally homogeneous silicate melt phase. They were then partially resorbed while hosted by the hydrosaline melt phase (e.g., Fig. 11f, h). At this stage, abundant quartz, topaz, zinnwaldite and ore minerals crystallized. Notably, most of the Sn that was originally present in the magma was carried in the hydrosaline melt to the margin of the dike, where cassiterite precipitated.

6.2. Comparison of ore mineral assemblages in the ongonites and topazite

The common accessory minerals in the No. 431 dike are columbite–tantalite, tapiolite, microlite, uraninite, rutile, hubnerite–ferberite, and zircon. Details of the distribution of the main ore minerals in the different rock types are provided in Table 7.

Table 7.

Summary of distribution of ore minerals in different rock types in the Xianghualing No. 431 dike.

	Sample no.	Columbite-group minerals	Tapiolite	Microlite	Cassiterite
	ZK840-11	+ + +	+ +	+ +	−
	ZK840-12	+ + +	+ +	+ +	−
Lower ongonite	ZK840-14	+ +	−	+	−
	ZK840-15	+ +	−	−	−
	ZK840-16	+ + +	−	−	−

	Sample no.	Columbite-group minerals	Tapiolite	Microlite	Cassiterite
	ZK840-20	+ +	−	−	−
	XXL-33	+ +	−	+ +	+
	XXL-34	+ +	−	−	+
Upper ongonite					
	XHL-310	+	−	−	+
	XHL-73	+	−	−	−
	XXL-08	+	−	+	+ +
	XXL-10	+ +	−	+	+ + +
Topazite					
	XXL-11	+	−	−	+ + +
	XXL-12	+	−	−	+ + +

Note: +++: most frequent; ++: more abundant; +: relatively abundant; −: rare or absent.

As shown by the mineralogical descriptions, the ongonites and topazite in the No. 431 dike display distinct Nb–Ta–Sn oxide mineral associations. In the ongonite of the lower dike, rare-metal elements are dominated by columbite–tantalite, together with tapiolite and microlite, but are free of cassiterite. Commonly, the subhedral Ta-poor columbite-(Mn) crystals are intergrown with rock-forming minerals, and they may indicate early magmatic crystallization. The progressive zoning in columbite-(Mn), comprising an increase in the Ta content from core to rim, can be attributed to the gradual differentiation of the magma. The experimental work of Linnen and Keppler (1997) and Linnen, 1998 and Linnen, 2004 suggests that the solubility of the Ta-rich end-member is higher than that of the Nb-rich member of columbite in peraluminous granites or pegmatite melts, similar to the relationship between the Fe-rich members relative to the Mn-rich members. Therefore, the coexisting tapiolite and tantalite-(Fe) represent the products of late-stage magmatic or possibly deuteric hydrothermal crystallization. Tapiolite is commonly found in pegmatites and granites that have undergone a highly evolved magmatic process (Beurlen et al., 2008, Černý et al., 1989a, Černý et al., 1989b, Chudik et al., 2008, Novák et al., 2003, Rao et al., 2009, Wang et al., 1997 and Zhang et al., 2004), and the fact that the tapiolite–tantalite pair plot at the appropriate boundary of the miscibility gap can probably be attributed to exsolution from an unstable homogeneous precursor (Černý et al., 1989a and Černý et al., 1989b). Fluorite is usually present in the mineral assemblage of tapiolite, tantalite, and microlite, suggesting crystallization from an F-rich liquid. Overall, the variations in the composition of columbite–tantalite and tapiolite reflect a highly differentiated and relatively Fe-richer magma system.

In the ongonite of the upper dike, columbite-(Mn) also occurs, and it is associated with a small amount of cassiterite. In the topazite that coexists with ongonite in the upper dike, Nb–Ta oxide minerals become less abundant, but their composition is similar to those in the coexisting ongonite. Interestingly, there is an abundance of Nb–Ta oxide minerals in the ongonite, but a large amount of cassiterite only appears in the topazite. In particular, the

cassiterite occurs as two distinct types. First, subhedral grains of cassiterite are associated with zircon and hubnerite (Fig. 10a), which may have crystallized from a melt phase; second, abundant, highly anhedral cassiterites with very fine-grained inclusion of topaz and varlamoffite in cavities may have crystallized at a later stage from an epigenetic hydrothermal fluid.

6.3. Differentiated Nb–Ta–Sn mineralization in the ongonites and topazite of the No. 431 dike

Granitic rocks rich in the rare elements are generally strongly enriched in F, and they are characterized by the crystallization of Nb–Ta–Sn ores, which may be directly linked to magmatic processes. Typical examples are found in the Beauvoir granite of the French Massif Central (Cuney et al., 1992 and Wang et al., 1992), in the Yichun granite of Southern China (Belkasmi et al., 2000 and Huang et al., 2002), and in the Czeck Podlesí granite (Breiter et al., 2007). It is particularly noted that Nb–Ta–Sn ores may be deposited at various stages of differentiation as coexisting columbite–tantalite and cassiterite are commonly disseminated in various facies of these granites. However, cassiterite may also be deposited in hydrothermal quartz veins, whereas columbite–tantalite is never found in such veins. In this study of the Xianghualing No. 431 dike, it was noted that the dike has two distinct types of rare-mental mineralization: Nb–Ta mineralization in the ongonites and Sn mineralization in the topazite. This apparently contrasting feature of Nb–Ta versus Sn mineralization differs from what is found in granites that are similarly enriched in rare-elements, and the difference may possibly be linked specifically to the highly F-enriched, high-level or near-surface emplacement of the Xianghualing Nb–Ta–Sn-enriched melt that permitted the efficient segregation of aluminosilicate and hydrosaline melts. As mentioned above, the ongonites of No. 431 dike are thought to be the product of extreme fractional crystallization of an F-rich granitic magma and unmixing of a silicate and fluoride-rich melt phases. The ore elements were likely present in the melt as complexes of TaF_8^{3-}, NbF_7^{2-}, and SnF_6^{2-}. The solubility of Nb, Ta, and Sn in the high-F fluids was maintained for a long time. At 600 °C, 120–490 ppm Nb is required for columbite saturation in a melt with 2 wt.% F (Linnen, 1998 and Linnen and Keppler, 1997). Simultaneously, the Nb- and Ta-complexes are sensitive to the Li-content in the melt. Breiter et al. (2007) confirmed that columbite often crystallized immediately after Li-mica (zinnwaldite), while the Li-contents decreased rapidly. As a result of both factors, the complexes of Nb and Ta were depolymerized easily, and the Nb–Ta minerals began to precipitate early from the ongonite melt. However, Bhalla et al. (2005) observed an increase in cassiterite solubility with increasing F in peraluminous melts. Obviously, the crystallization of abundant topaz in the ongonites and topazite would have rapidly caused a decrease in the activity of F in the melt. As a result, the cassiterite could crystallize during the post-magmatic and hydrothermal stages, and even varlamoffite could form in the cavities. Therefore, the increase in the F content of the melt that produced the No. 431 dike would inevitably have led to tin mineralization in the strongly F-enriched topazitic melts.

The observed trends of increasing Fe in columbite group minerals in ongonite of the lower dike as compared to increasing Mn in columbite group minerals in ongonite and topazite of the upper dike (Fig. 12; Table 4) reflect a decrease of whole-rock FeO_t/MnO value from lower to upper part of the dike (Table 1). The compositional trends of the columbite minerals also concur with Mn-poor zinnwaldite in lower ongonite and Mn-bearing zinnwaldite in upper ongonite and topazite (Table 3). We therefore interpret the two different compositional trends shown in Fig. 12 to reflect the overall increase of differentiation from lower to upper parts in the dike.

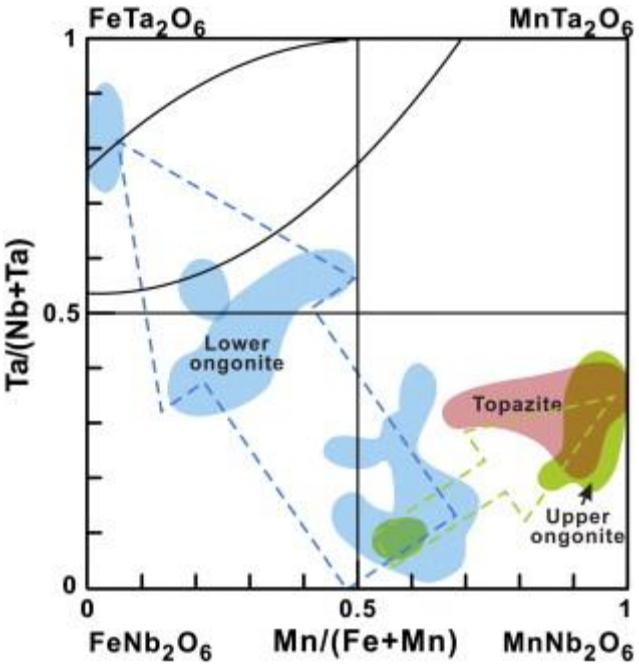

Fig. 12. : Fractionation trends of the columbite-group minerals and tapiolite from the No. 431 dike. Arrows indicate direction of compositional fractionation.

6.4. A possible mechanism for the segregation of aluminosilicate and hydrosaline melts in the No. 431 dike

Aluminosilicate-dominated and hydrosaline melt phases as those inferred to have crystallized ongonite and topazite of the No. 431 dike differ in density and viscosity. Hydrosaline melts have low densities and low viscosities compared to aluminosilicate-dominated melts (Badanina et al., 2004, Peretyazhko, 2010, Veksler, 2004 and Veksler and Thomas, 2002), and the density contrast of the two melt phases could thus have caused segregation of the hydrosaline melt into structurally higher positions. However, the zoning of both lower ongonite from core to margin (as revealed in drill core) as well as upper ongonite to topazite (as exposed in the exploratory trench) suggests that the hydrosaline melt separated toward both – the upper and the lower – dike margins, which cannot be explained by simple density-driven segregation. Temperature gradients between dike interior and country rocks could have also affected the segregation of the two melt phases. However, if temperature was the main driving force for segregation we would expect that the least evolved ongonite rocks would have crystallized along the colder dike margins and the more evolved ongonite rocks and topazite would have crystallized in the dike interior.

Another possible explanation – and our preferred interpretation – is that continued dike propagation/widening caused the partial (in subsurface ongonite) to significant (from near-surface ongonite to topazite) segregation of hydrosaline from aluminosilicate melt. Elastic propagation rates for fractures exceed viscous flow rates of silicate magmas (e.g., Clarke et al., 1998 and Rubin, 1993), and dike propagation/widening will therefore create a pressure gradient and may shortly create a vacuum. The least viscous material of the dike – the hydrosaline melt – will have been instantly drawn into the low-pressure zone, and thereby largely separated from the aluminosilicate melt. The greater width of the dike as exposed in the exploratory trench relative to the drill core could reflect that the dike opened further at this structurally higher position, which caused a more advanced segregation of the two melt

phases into ongonite and topazite in the upper dike than at the structurally lower position with zoned subsurface ongonite.

We believe that there might be records in the rocks such as melt inclusions of two immiscible melts, which may be present in minerals from both types of rocks and can be good for further studies. A detailed investigation of melt inclusions from the different mineral types and crystal populations will be ideally suited to test – and to refine – our proposed model. However, the detailed compositional and textural study presented here is an important guide for the sensible collection and interpretation of such data.

7. Conclusions

The Xianghualing No. 431 dike is composed of ongonite and topazite which are predominantly mineralized by Nb- and Ta-bearing and Sn-bearing ore minerals, respectively. Ongonite crystallized from an aluminosilicate magma that reached saturation in F and other volatile components. Upon exsolution of a hydrosaline melt phase (or phases), the aluminosilicate melt rapidly crystallized to a quartz-, K-feldspar-, and albite-dominated assemblage with Nb–Ta ore minerals of the columbite–tantalite, tapiolite and microlite as characteristic accessories. Topazite formed from the hydrosaline melt that segregated toward the margin of the small-scale dike, crystallizing a topaz-, zinnwaldite-, and quartz-dominated assemblage. Exsolution of the two melt phases and their efficient segregation into core and rim zones of the dike may have been driven by dike propagation/widening subsequent to the initial dike emplacement. Melt inclusions should provide a detailed record of the proposed evolution and further provide compositional details on the fractionating liquids.

Acknowledgments

This study was supported financially by the Natural Science Foundation of China (Grant Nos. 41230315 and 41172061), the National Key Basic Research Program of China (973 Program) (No. 2012CB416704), and the Key Research Project of the China Geological Survey (Grant No. 12120113067300). We thank Dr. W.L. Zhang and Mr. B. Wu for their kind assistance with the laboratory work, Mr. X.G. Luo and Mr. T. Ding for their help in the field work. We greatly appreciated the comments by the guest editor Dr. M.F. Zhou, and two reviewers, Dr. K. Breiter and Dr. T.P. Zhao, which helped to considerably improve the manuscript.

References

Anders and Grevesse, 1989
E. Anders, N. Grevesse
Abundances of the elements: meteoritic and solar
Geochim. Cosmochim. Acta, 53 (1989), pp. 197–214

Badanina et al., 2004
E.V. Badanina, I.V. Veksler, R. Thomas, L.F. Syritso, R.B. Trumbull
Magmatic evolution of Li–F, rare-metal granites: a case study of melt inclusions in the Khangilay complex, Eastern Transbaikalia (Russia)
Chem. Geol., 210 (2004), pp. 113–133

Belkasmi et al., 2000
M. Belkasmi, M. Cuney, P.J. Pollard, A. Bastoul

Chemistry of the Ta–Nb–Sn–W oxide minerals from the Yichun rare metal granite (SE China): genetic implications and comparison with Moroccan and French Hercynian examples
Mineral. Mag., 64 (2000), pp. 507–523

Beurlen et al., 2008
H. Beurlen, M.R. Da Silva, R. Thomas, D.R. Soares, P. Olivier
Nb–Ta–(Ti–Sn) oxide mineral chemistry as tracer of rare-element granitic pegmatite fractionation in the Borborema Province, Northeastern Brazil
Mineral. Deposita, 43 (2008), pp. 207–228

Bhalla et al., 2005
P. Bhalla, F. Holtz, R.L. Linnen, H. Behrens
Solubility of cassiterite in evolved granitic melts: effect of T, fO_2, and additional volatiles
Lithos, 80 (2005), pp. 387–400

Breiter, 2012
K. Breiter
Nearly contemporaneous evolution of the A- and S-type fractionated granites in the Krušné hory/Erzgebirge Mts., Central Europe
Lithos, 151 (2012), pp. 105–121

Breiter et al., 2005
K. Breiter, A. Müller, J. Leichmann, A. Gabašová
Textural and chemical evolution of a fractionated granitic system: the Podlesí stock, Czech Republic
Lithos, 80 (2005), pp. 323–345

Breiter et al., 2007
K. Breiter, R. Škoda, P. Uher
Nb–Ta–Ti–W–Sn-oxide minerals as indicators of a peraluminous P- and F-rich granitic system evolution: Podlesí, Czech Republic
Mineral. Petrol., 91 (2007), pp. 225–248

Burt, 1992
D.M. Burt
Lunar mining of oxygen using fluorine
The Second Conf. on Lunar Bases and Space Activities of the 21st Century, 1 (1992), pp. 423–428

Černý, 1989
P. Černý
Characteristics of pegmatite deposits of tantalum
‚in: P. Möller, P. Černý, F. Saupé (Eds.), Lanthanides, Tantalum and Niobium, Special Publication No. 7 of the Society for Geology Applied to Mineral Deposits (1989), pp. 195–239

Černý and Ercit, 1989
P. Černý, T.S. Ercit

Mineralogy of niobium and tantalum: crystal chemical relationships, paragenetic aspects and their economic implications
‚in: P. Möller, P. Černý, F. Saupé (Eds.), Lanthanides, Tantalum and Niobium, Special Publication No. 7 of the Society for Geology Applied to Mineral Deposits (1989), pp. 27–79

Černý et al., 1989a
P. Černý, R. Chapman, L.E. Chackowsky, T.S. Ercit
A ferrotantalite–ferrotapiolite intergrowth from Spittal ad Drau, Carinthia, Austria
Mineral. Petrol., 41 (1989), pp. 53–63

Černý et al., 1989b
P. Černý, E.K. Ucakuwun, R. Chapman
A ferrotantalite–ferrotapiolite exsolution from Uganda
Neues Jb. Mineral. Monat., 3 (1989), pp. 109–120

Černý et al., 1992
P. Černý, T.S. Ercit, M.A. Wise
The tantalite–tapiolite gap: natural assemblages versus experimental data
Can. Mineral., 30 (1992), pp. 587–596

Chen, 1984
D.Q. Chen
On the characteristics and genesis of topaz–felsite porphyry
Acta Petrol. Mineral., 1 (1984), pp. 9–17 (in Chinese with English abstract)

Chudik et al., 2008
P. Chudik, P. Uher, M. Kohut, P. Bačík
Accessory columbite to tantalite, tapiolite and zircon: products of extreme fractionation in highly peraluminous pegmatitic granite from the Povžaský Inovec Mountains, Western Carpathians, Slovakia
J. Geosci., 53 (2008), pp. 323–334

Clarke et al., 1998
D.B. Clarke, A.S. Henry, M.A. White
Exploding xenoliths and the absence of ‘elephants’ graveyards in granite batholiths
J. Struct. Geol., 20 (1998), pp. 1325–1343

Cobbing et al., 1986
E.J. Cobbing, D.I.J. Mallick, P.E.J. Pitfield, L.H. Teoh
The granites of the Southeast Asian tin belt
J. Geol. Soc., 143 (1986), pp. 537–550

Cuney et al., 1992
M. Cuney, C. Marignac, A. Weisbrod
The Beauvoir topaz–lepidolite albite granite (Massif Central, France); the disseminated magmatic Sn–Li–Ta–Nb–Be mineralization
Econ. Geol., 87 (1992), pp. 1766–1794

Du and Huang, 1984

S.H. Du, Y.H. Huang
Investigation on Xianghualingite
Sci. China B, 11 (1984), pp. 1039–1047 (in Chinese with English abstract)

Eadington and Nashar, 1978
P.J. Eadington, B. Nashar
Evidence for the magmatic origin of quartz–topaz rocks from the New England Batholith, Australia
Contrib. Mineral. Petrol., 67 (1978), pp. 433–438

Fenn, 1977
P.M. Fenn
The nucleation and growth of alkali feldspars from hydrous melts
Can. Mineral., 15 (1977), pp. 135–161

Foster, 1960a
M.D. Foster
Interpretation of the composition of trioctahedral micas
U. S. Geol. Surv. Prof. Pap., 354-B (1960), pp. 11–49

Foster, 1960b
M.D. Foster
Interpretation of the composition of lithium micas
U. S. Geol. Surv. Prof. Pap., 354-E (1960), pp. 115–147

Gioncada et al., 2014
A. Gioncada, P. Orlandi, L. Vezzoli, R.H. Omarini, R. Mazzuoli, V. Lopez-Azarevich, J. Ruch
Topaz magmatic crystallization in rhyolites of the Central Andes (Chivinar volcanic complex, NW Argentina): constraints from texture, mineralogy and rock chemistry
Lithos, 184 (2014), pp. 62–73

Helba et al., 1997
H. Helba, R.B. Trumbull, G. Morteani, S.O. Khalil, A. Arslan
Geochemical and petrographic studies of Ta mineralization in the Nuweibi albite granite complex, Eastern Desert, Egypt
Mineral. Deposita, 32 (1997), pp. 164–179

Hersum and Marsh, 2007
T.G. Hersum, B.D. Marsh
Igneous textures: on the kinetics behind the words
Elements, 3 (2007), pp. 247–252

Hogarth, 1977
D.D. Hogarth
Classification and nomenclature of the pyrochlore group
Am. Mineral., 62 (1977), pp. 403–410

Huang et al., 1958
W.H. Huang, S.H. Tu, K.H. Wang, C.L. Chao, C.C. Yu
Hsiang-hua-shih, a new beryllium mineral

Ti-Chih-yueh-K'an, 7 (1958), p. 35 ((in Chinese). New mineral name introduced in American Mineralogist 1959, 44, 1327–1328)

Huang et al., 1988
Y.H. Huang, S.H. Du, X.Z. Zhou
Xianghualing Rocks, Mineral Deposits and Minerals
Science and Technology Press, Beijing (1988), pp. 1–255 (in Chinese with English abstract)

Huang et al., 2002
X.L. Huang, R.C. Wang, X.M. Chen, H. Hu, C.S. Liu
Vertical variations in the mineralogy of the Yichun topaz–lepidolite granite, Jiangxi Province, southern China
Can. Mineral., 40 (2002), pp. 1047–1068

Johnston and Chappell, 1992
C. Johnston, B.W. Chappell
Topaz-bearing rocks from Mount Gibson, North Queensland, Australia
Am. Mineral., 77 (1992), pp. 303–313

Kamenetsky and Kamenetsky, 2010
V.S. Kamenetsky, M.B. Kamenetsky
Magmatic fluids immiscible with silicate melts: examples from inclusions in phenocrysts and glasses, and implications for magma evolution and metal transport
Geofluids, 10 (2010), pp. 293–311

Kortemeier and Burt, 1988
W.T. Kortemeier, D.M. Burt
Ongonite and topazite dikes in the Flying W ranch area, Tonto basin, Arizona
Am. Mineral., 73 (1988), pp. 507–523

Kovalenko and Kovalenko, 1976
V.I. Kovalenko, N.I. Kovalenko
Ongonite (Topaz-bearing Quartz Keratophyre)-Subvolcanic Analogue of Rare-metal Li–F Granite
Nauka Press, Moscow (1976), p. 128 (in Russian)

Kovalenko et al., 1971
V.I. Kovalenko, M.I. Kuzmin, V.S. Antipin, L.L. Petrov
Topaz-bearing quartz keratophyre (ongonite), a new variety of subvolcanic igneous vein rock
Dokl. Acad. Sci. USSR Earth Sci. Sect., 199 (1971), pp. 132–134

Kovalenko et al., 1975
V.I. Kovalenko, A.M. Grebennikov, V.S. Antipin
Ongonite of the Arybulak stock, Transbaikal: the first find of a subvolcanic analog of rare metal-bearing lithium-fluorine granite (apogranite) in the USSR
Dokl. Acad. Sci. USSR Earth Sci. Sect., 220 (1975), pp. 158–160 (translated from Doklady Akademii Nauk SSSR, 220, No. 5, 1169–1171)

Linnen, 1998
R.L. Linnen
The solubility of Nb–Ta–Zr–Hf–W in granitic melts with Li and Li + F; constraints for mineralization in rare metal granites and pegmatites
Econ. Geol., 93 (1998), pp. 1013–1025

Linnen, 2004
R.L. Linnen
Ferrocolumbite–manganotantalite trends in granites and pegmatites: experimental and natural constraints
Geol. Soc. Am. Abstr. Programs, 36 (5) (2004), p. 115

Linnen and Keppler, 1997
R.L. Linnen, H. Keppler
Columbite solubility in granitic melts: consequences for the enrichment and fractionation of Nb and Ta in the Earth's crust
Contrib. Mineral. Petrol., 128 (1997), pp. 213–227

Liu et al., 1996
C.S. Liu, W.Z. Shen, D.Z. Wang
The characteristics and genetic mechanism of igneous topazites in South China
Acta Geol. Sin., 9 (1996), pp. 33–45

London and Morgan, 2012
D. London, G.B. Morgan
The pegmatite puzzle
Elements, 8 (2012), pp. 263–268

Mo et al., 1980
S.Z. Mo, B.D. Ye, W.Z. Pang, S.N. Wan
Granitoid Geology in the Nanling Region
Geological Publishing House, Beijing (1980), pp. 115–180

Monier and Robert, 1986
G. Monier, J.L. Robert
Evolution of the miscibility gap between muscovite and biotite solid solutions with increasing lithium content: an experimental study in the system K_2O–Li_2O–MgO–FeO–Al_2O_3–SiO_2–H_2O–HF
Mineral. Mag., 50 (1986), pp. 641–651

Neiva, 1996
M.R. Neiva
Geochemistry of cassiterite and its inclusion and exsolution products from tin and tungsten deposits in Portugal
Can. Mineral., 34 (1996), pp. 745–768

Novák et al., 2003
M. Novák, P. Černý, P. Uher
Extreme variation and apparent reversal of Nb–Ta fractionation in columbite-group minerals from the Scheibengraben beryl-columbite granitic pegmatite, Maršíkov, Czech Republic

Eur. J. Mineral., 15 (2003), pp. 565–574

Peretyazhko, 2010
I.S. Peretyazhko
Genesis of mineralized cavities (miaroles) in granitic pegmatites and granites
Petrology, 18 (2010), pp. 183–208

Peretyazhko et al., 2007
I.S. Peretyazhko, V.Y. Zagorsky, E.A. Tsareva, A.N. Sapozhnikov
Immiscibility of calcium fluoride and aluminosilicate melts in ongonite from the Ary-Bulak intrusion, Eastern Transbaikal region
Dokl. Earth Sci., 413 (2007), pp. 315–320

Pichavant et al., 1987
M. Pichavant, J.V. Herrera, S. Boulmier, L. Briqueu, J.L. Joron, M. Juteau, M. Vernet
The Macusani glasses, SE Peru: evidence of chemical fractionation in peraluminous magmas
B.O. Mysen (Ed.), Magmatic Processes: Physicochemical Principles (1987), pp. 359–373

Pietro, 2008
A. Pietro
Decryption of igneous rock textures: crystal size distribution
Rev. Mineral. Geochem., 69 (2008), pp. 623–649

Pollard, 1989
P.J. Pollard
Geologic characteristics and genetic problems associated with the development of granite-hosted deposits of tantalum and niobium
‚in: P. Möller, P. Černý, F. Saupé (Eds.), Lanthanides, Tantalum and Niobium, Special Publication No. 7 of the Society for Geology Applied to Mineral Deposits in Lanthanides, Tantalum and Niobium, Springer, Berlin Heidelberg (1989), pp. 240–256

Qi et al., 2000
L. Qi, J. Hu, G. D.Conrad
Determination of trace elements in granites by inductively coupled plasma mass spectrometry
Talanta, 51 (2000), pp. 507–513

Raimbault and Burnol, 1998
L. Raimbault, L. Burnol
The Richemont rhyolite dike, Massif Central, France; a subvolcanic equivalent of rare-metal granites
Can. Mineral., 36 (1998), pp. 265–282

Rao et al., 2009
C. Rao, R.C. Wang, H. Hu, W.L. Zhang
Complex internal textures in oxide minerals from the Nanping No. 31 dike of granitic pegmatite, Fujian province, southeastern China
Can. Mineral., 47 (2009), pp. 1195–1212

Roedder, 1992
E. Roedder
Fluid inclusion evidence for immiscibility in magmatic differentiation
Geochim. Cosmochim. Acta, 56 (1992), pp. 5–20

Roedder and Coombs, 1967
E. Roedder, D.S. Coombs
Immiscibility in granitic melts, indicated by fluid inclusions in ejected granitic blocks from Ascension Island
J. Petrol., 8 (1967), pp. 417–451

Rubin, 1993
A.M. Rubin
Tensile fracture of rock at high confining pressure: implications for dike propagation
J. Geophys. Res., 98 (1993), pp. 15919–15935

Shchekina et al., 2013
T.I. Shchekina, E.N. Gramenitskiy, Y.O. Alferyeva
Leucocratic magmatic melts with the maximum fluorine concentrations: experiment and relations in nature
Petrology, 21 (2013), pp. 457–470

Štemprok, 1991
M. Štemprok
Ongonite from Ongon Khairkhan, Mongolia
Mineral. Petrol., 43 (1991), pp. 255–273

Štemprok et al., 2008
M. Štemprok, D. Dolejš, A. Müller, R. Seltmann
Textural evidence of magma decompression, devolatilization and disequilibrium quenching: an example from the Western Krušné hory/Erzgebirge granite pluton
Contrib. Mineral. Petrol., 155 (2008), pp. 93–109

Swanson, 1977
S.E. Swanson
Relation of nucleation and crystal-growth rate to the development of granitic textures
Am. Mineral., 62 (1977), pp. 966–978

Takahashi et al., 2002
Y. Takahashi, H. Yoshida, N. Sato, K. Hama, Y. Yusa, H. Shimizu
W- and M-type tetrad effects in REE patterns for water–rock systems in the Tono uranium deposit, central Japan
Chem. Geol., 184 (2002), pp. 311–335

Taylor, 1992
R.P. Taylor

Petrological and geochemical characteristics of the Pleasant Ridge zinnwaldite-topaz granite, southern New Brunswick, and comparisons with other topaz-bearing felsic rocks
Can. Mineral., 30 (1992), pp. 895–921

Tindle and Breaks, 1998
A.G. Tindle, F.W. Breaks
Oxide minerals of the Separation Rapids rare-element granitic pegmatite group, northwestern Ontario
Can. Mineral., 36 (1998), pp. 609–635

Tindle and Webb, 1990
A.G. Tindle, P.C. Webb
Estimation of lithium contents in trioctahedral micas using microprobe data: application to micas from granitic rocks
Eur. J. Mineral., 2 (1990), pp. 595–610

Veksler, 2004
I.V. Veksler
Liquid immiscibility and its role at the magmatic–hydrothermal transition: a summary of experimental studies
Chem. Geol., 210 (2004), pp. 7–31

Veksler and Thomas, 2002
I.V. Veksler, R. Thomas
An experimental study of B-, P- and F-rich synthetic granite pegmatite at 0.1 and 0.2 GPa
Contrib. Mineral. Petrol., 143 (2002), pp. 673–683

Veksler et al., 2012
I.V. Veksler, A.M. Dorfman, P. Dulski, V.S. Kamenetsky, L.V. Danyushevsky, T. Jeffries, D.B. Dingwell
Partitioning of elements between silicate melt and immiscible fluoride, chloride, carbonate, phosphate and sulfate melts, with implications to the origin of natrocarbonatite
Geochim. Cosmochim. Acta, 79 (2012), pp. 20–40

Wang et al., 1992
R.C. Wang, F. Fontan, P. Monchoux
Mineraux dissemines comme indicateurs du caractere pegmatitique du granite de Beauvoir, Massif d'Echassieres, allier, France
Can. Mineral., 30 (1992), pp. 763–770

Wang et al., 1997
R.C. Wang, F. Fontan, S.J. Xu, X.M. Chen, P. Monchoux
The association of columbite, tantalite and tapiolite in the Suzhou granite, China
Can. Mineral., 35 (1997), pp. 699–706

Xie et al., 2013
L. Xie, R.C. Wang, J. Chen, J.C. Zhu, W.L. Zhang, J.J. Lu, R.Q. Zhang

A tin-mineralized topaz rhyolite dike with coeval topaz granite enclaves at Qiguling in the Qitianling tin district, southern China
Lithos, 170 (2013), pp. 252–268

Yuan et al., 2007
S.D. Yuan, J.T. Peng, N.P. Shen, R.Z. Hu, T.M. Dai
^{40}Ar–^{39}Ar isotopic dating of the Xianghualing Sn-polymetallic orefield in Southern Hunan, China and its geological implications
Acta Geol. Sin., 81 (2007), pp. 278–286 (English Edition)

Yuan et al., 2008
S.D. Yuan, J.T. Peng, R.Z. Hu, H.M. Li, N.P. Shen, D.L. Zhang
A precise U–Pb age on cassiterite from the Xianghualing tin-polymetallic deposit (Hunan, South China)
Mineral. Deposita, 43 (2008), pp. 375–382

Zhang et al., 2004
A.C. Zhang, R.C. Wang, H. Hu, H. Zhang, J.C. Zhu, X.M. Chen
Chemical evolution of Nb–Ta oxides and zircon from the Koktokay No. 3 granitic pegmatite, Altai, northwestern China
Mineral. Mag., 68 (2004), pp. 739–756

Zhu and Liu, 1990
J.C. Zhu, W.X. Liu
Topazite–ongonite relationship and its bearing on vertical zonation in rare-metal granites: evidence from Xianghualing District, Hunan Province, China
Proceedings of the Eighth Quadrennial IAGOD Symposium, VI (1990), pp. 303–313

Zhu et al., 1993
J.C. Zhu, W.X. Liu, F.Y. Zhou
Ongonite and topazite in dike No. 431 of Xianghualing district and their spatial zonation and genetic relationship
Acta Petrol. Sin., 9 (1993), pp. 158–166 (in Chinese with English abstract)

Zhu et al., 2001
J.C. Zhu, R.K. Li, F.C. Li, X.L. Xiong, F.Y. Zhou, X.L. Huang
Topaz–albite granites and rare-metal mineralization in the Limu district, Guangxi Province, southeast China
Mineral. Deposita, 36 (2001), pp. 393–405

Zhu et al., 2011
J.C. Zhu, R.C. Wang, J.J. Liu, H. Zhang, W.L. Zhang, L. Xie, R.Q. Zhang
Fractionation, evolution, petrogenesis and mineralization of Laiziling Granite Pluton, Southern Hunan Province
Geol. J. China Univ., 17 (2011), pp. 381–392 (in Chinese with English abstract)